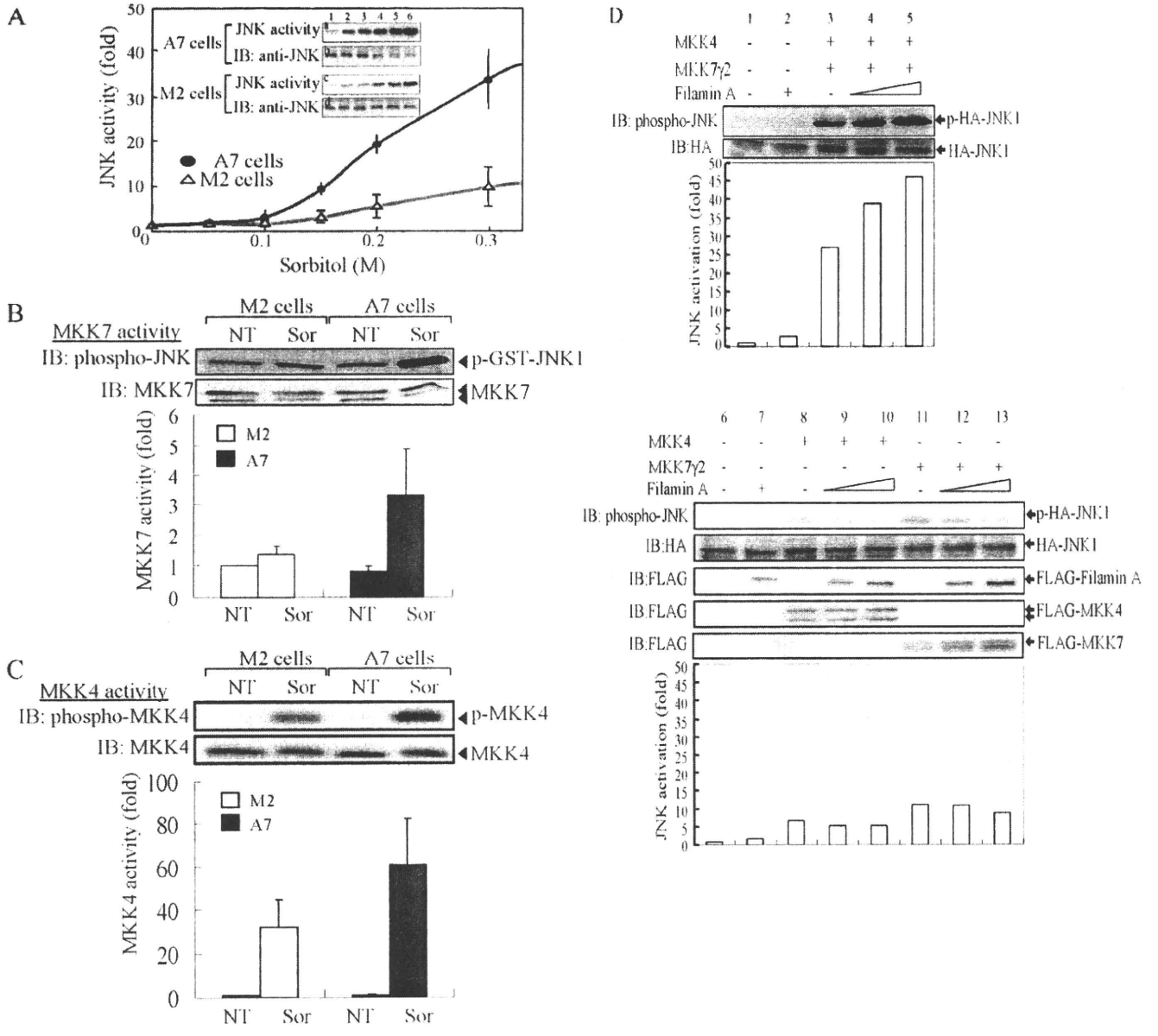

Figure 5 Impaired synergistic JNK activation in Filamin-A-deficient cells

(**A**) Inset: confluent M2 and A7 human melanoma cells were treated with sorbitol (0.05, 0.1, 0.15, 0.2 or 0.3 M in lanes 1–6 respectively) at 37 °C for 20 min. Lysates were immunoprecipitated with anti-JNK Ab, and JNK activity in the immunoprecipitates was measured using an *in vitro* kinase assay with GST–c-Jun as the substrate. ^{32}P-labelled phosphorylated GST–c-Jun (panels a and c) and total immunoprecipitated JNK (panels b and d) are shown. Graph: levels of JNK activity in treated M2 (△) and A7 (●) cells were expressed as the fold-stimulation compared with levels in untreated M2 or A7 cells. (**B**) Confluent M2 and A7 cells were treated with 0.5 M sorbitol at 37 °C for 20 min, and lysates were immunoprecipitated with an anti-MKK7 mAb. MKK7 activity in the immunoprecipitates was measured using an *in vitro* kinase assay with GST–JNK1 as the substrate. Levels of phosphorylated JNK were determined using an anti-phospho-JNK Ab (upper panel). Total immunoprecipitated MKK7 was determined using an anti-MKK7 Ab (lower panel). Histogram: MKK7 activity in lysates of M2 cells and A7 cells that were not treated (NT) or treated with 0.5 M sorbitol (Sor) were expressed relative to activities of NT in M2 cells. Bars indicate the means ± S.E.M. for three independent experiments. (**C**) MKK4 activity was measured using an anti-phospho-MKK4 (upper panel) Ab. Total MKK4 was determined using an anti-MKK4 Ab (lower panel). Histogram: MKK4 activity in lysates of M2 cells and A7 cells that were not treated (NT) or treated with 0.5 M sorbitol (Sor) were expressed relative to activities of NT in M2 cells as described in (**B**). (**D**) M2 cells were co-transfected with various amounts of pCMV5/FLAG-Filamin A (0, 1, 0, 0.5 and 1 μg in lanes 1–5 respectively) and 0.5 μg of pCMV5/HA-JNK1, together with (lanes 1 and 2) 0.5 μg of pCMV5/FLAG-MKK4 and FLAG-MKK7γ2. M2 cells were co-transfected with various amounts of pCMV5/FLAG-Filamin A (0, 0.5 and 1 μg in lanes 8–10 and 11–13 respectively) and 0.5 μg of pCMV5/HA-JNK1, with 0.5 μg of pCMV5/FLAG-MKK4 (lanes 8–10) or 0.5 μg of pCMV5/FLAG-MKK7γ2 (lanes 11–13). After 48 h culture, cell lysates were analysed for JNK phosphorylation (activation) by immunoblotting with anti-phospho-JNK Ab. Total HA–JNK1, FLAG–Filamin A, FLAG–MKK4 and FLAG–MKK7 expressions were determined using anti-HA and anti-FLAG Abs. Histogram: densitometry of the bands in the upper panel, expressed as the fold increase over phosphorylation in the absence of MKK4, MKK7 proteins and Filamin A. After 48 h culture, cell lysates were analysed for JNK phosphorylation (activation) by immunoblotting with anti-phospho-JNK Ab. Total HA–JNK1 expression was determined using anti-HA Abs. Histogram: densitometry of the bands in the upper panel, expressed as the fold increase over phosphorylation in the absence of MKK4, MKK7 proteins and Filamin A. Results were obtained from at least three independent experiments. IB, immunoblot.

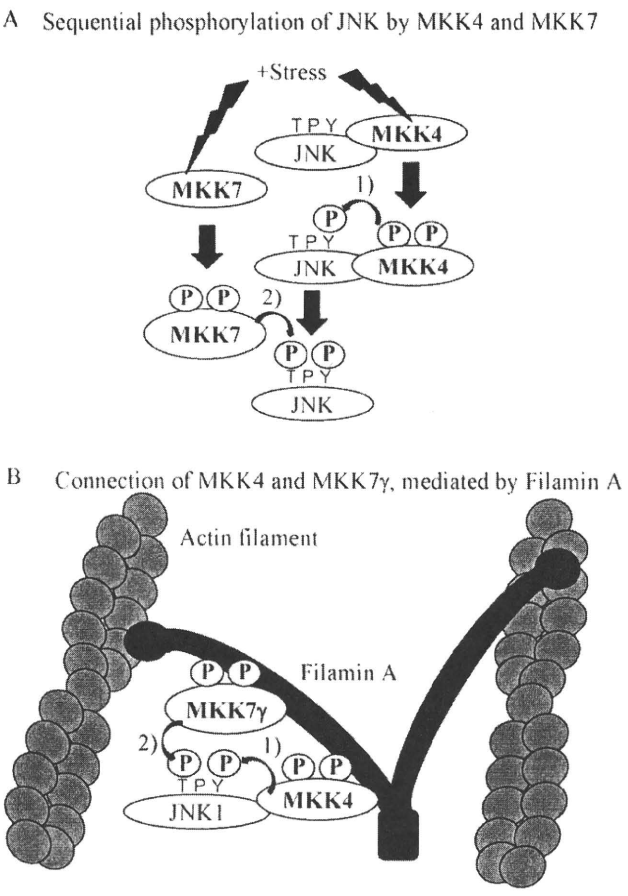

Figure 6 Schematic model of the role of Filamin A in the sequential phosphorylation of JNK1 by MKK4 and MKK7γ

(**A**) Synergistic activation of JNK through sequential tyrosine/threonine phosphorylation by MKK4 and MKK7 in murine cells (as reported in our previous study; [7]). In a murine ES cell subjected to stress, activated (phosphorylated) MKK4 mediates the phosphorylation of the tyrosine residue of the threonine-proline-tyrosine motif (TPY) of JNK (step 1), followed by threonine phosphorylation of the same JNK molecule by activated (phosphorylated) MKK7 (step 2). JNK activity is synergistically enhanced. (**B**) MKK4 and MKK7γ are connected by their mutual interaction with Filamin A. As demonstrated in the present study, Filamin A associates with actin filaments comprising the cytoskeleton. Filamin A also contains distinct binding sites for MKK4 and MKK7, and can interact simultaneously with these MAPKKs. The interaction of all three proteins with JNK induces synergistic levels of JNK phosphorylation and thus activation.

(tumour necrosis factor)-receptor-associated factor]. TRAF2 is an intracellular adaptor protein that is involved in signal transduction from the TNF receptor and related receptors, and is required for TNF-induced JNK activation [12,17]. Other work has indicated that Filamin A binds to small GTPases such as Rac, Rho, Cdc42 and RalA [16]. Thus many signalling molecules, including small GTPases, TRAF2 and MKK4, accumulate on Filamin A. These observations suggest that, as well as regulating cytoskeletal architecture, Filamin A may function as a signalsome that connects diverse signalling pathways, including MAPK modules. Conversely, in addition to its role in stress signalling, JNK has been implicated in cell migration and cytoskeletal reorganization. Huang et al. [18] reported that JNK1 phosphorylates paxillin, a focal adhesion adaptor, both *in vitro* and in intact fish and rat cells. Similarly, Otto et al. [19] identified p150-Spir, a *Drosophila* JNK-interacting protein, as belonging to the Wiscott–Aldrich syndrome protein homology domain-2 family of proteins involved in actin reorganization. p150-Spir is phosphorylated by JNK both *in vitro* and *in vivo*, indicating that p150-Spir is a downstream target of JNK function and providing a direct link between JNK activity and actin reorganization. Thus the downstream targets of JNK include not only transcription factors, but also cytoskeletal regulators. Another intriguing observation is that the receptor tyrosine kinase Ror2 mediates Wnt5a-induced polarized cell migration by activating JNK via Filamin A [20]. Lastly, Filamin A is not the only Filamin family member involved in JNK signalling, as Filamin B functions as a scaffold linking activated Rac1, MEKK1 and MKK4 to JNK during type I interferon signalling [21,22]. Taken together, these data point towards multiple connections between signalling modules and Filamin proteins.

The present study has revealed interesting differences among MKK7 isoforms. Tournier et al. [13] showed that MKK7 isoforms are present both in the cytoplasm and the nucleus, and are selectively regulated by specific extracellular stimuli. We have previously reported that treatment of ES cells with sorbitol (which affects the plasma membrane) induces stronger activation of MKK7γ1 than MKK7α1 [6]. In the present study, we discovered that MKK7γ1 co-localizes with actin on stress fibres and with Filamin A at the cell surface (Figures 3A and 3B). On the other hand, we found that MKK7α1 and MKK7γ1 deletion B, neither of which can interact with Filamin A, were diffusely distributed throughout the cytoplasm (Figure 3C). These data suggest the possibility that MKK7γ1, which co-localizes with the actin cytoskeleton right up to the plasma membrane, is involved in signal transduction from this membrane, whereas MKK7α1, which is distributed throughout the cytoplasm, is involved in a cytoplasmic signalling pathway. Thus differences in the intracellular distribution of MKK7 isoforms may correspond to different MAPK signalling modules mediating distinct cellular responses.

In conclusion, the present study has demonstrated that Filamin A interacts with specific MKK7 isoforms and is a candidate for a presumed 'binder' protein needed to form the JNK–MKK4–MKK7 MAPK module. Filamin A may support or induce the sequential phosphorylation of JNK by MKK4 and MKK7, and thus function as a signalsome involved in cytoskeletal events. Future work will establish whether Filamin A is a key factor supporting additional JNK signalling cascades.

AUTHOR CONTRIBUTION

Kentaro Nakagawa, Misato Sugahara, Tokiwa Yamasaki and Hiroaki Kajiho performed the experiments. Shinya Takahashi and Jun Hirayama analysed the data. Yasuhiro Minami, Yasutaka Ohta and Toshio Watanabe provided essential reagents. Yutaka Hata, Toshiaki Katada and Hiroshi Nishina designed the experiments, provided funding and wrote the paper.

ACKNOWLEDGEMENTS

We are grateful to numerous members of the Nishina and Katada laboratories for helpful discussions, expert technical assistance and critical reading of this manuscript.

FUNDING

This work was supported, in part, by a Grant-in-Aid for Scientific Research on a Priority Area from the Ministry of Education, Culture, Sport, Science and Technology of Japan and the Ministry of Health, Labour and Welfare of Japan [grant numbers 17081005 and 20390022].

REFERENCES

1 Davis, R. J. (2000) Signal transduction by the JNK group of MAP kinases. Cell **103**, 239–252
2 Chang, L. and Karin, M. (2001) Mammalian MAP kinase signalling cascades. Nature **410**, 37–40
3 Lawler, S., Fleming, Y., Goedert, M. and Cohen, P. (1998) Synergistic activation of SAPK1/JNK1 by two MAP kinase kinases *in vitro*. Curr. Biol. **8**, 1387–1390

4 Fleming, Y., Armstrong, C. G., Morrice, N., Paterson, A., Goedert, M. and Cohen, P. (2000) Synergistic activation of stress-activated protein kinase 1/c-Jun N-terminal kinase (SAPK1/JNK) isoforms by mitogen-activated protein kinase kinase 4 (MKK4) and MKK7. Biochem. J. **352**, 145–154

5 Lisnock, J., Griffin, P., Calaycay, J., Franz, B., Parsons, J., O'Keefe, S. J. and LoGrasso, P. (2000) Activation of JNK3 α1 requires both MKK4 and MKK7: kinetic characterization of *in vitro* phosphorylated JNK3 α1. Biochemistry **39**, 3141–3148

6 Wada, T., Nakagawa, K., Watanabe, T., Nishitai, G., Seo, J., Kishimoto, H., Kitagawa, D., Sasaki, T., Penninger, J. M., Nishina, H. and Katada, T. (2001) Impaired synergistic activation of stress-activated protein kinase SAPK/JNK in mouse embryonic stem cells lacking SEK1/MKK4: different contribution of SEK2/MKK7 isoforms to the synergistic activation. J. Biol. Chem. **276**, 30892–30897

7 Kishimoto, H., Nakagawa, K., Watanabe, T., Kitagawa, D., Momose, H., Seo, J., Nishitai, G., Shimizu, N., Ohata, S., Tanemura, S. et al. (2003) Different properties of SEK1 and MKK7 in dual phosphorylation of stress-induced activated protein kinase SAPK/JNK in embryonic stem cells. J. Biol. Chem. **278**, 16595–16601

8 Nishina, H., Wada, T. and Katada, T. (2004) Physiological roles of SAPK/JNK signaling pathway. J. Biochem. **136**, 123–126

9 Nishitai, G., Shimizu, N., Negishi, T., Kishimoto, H., Nakagawa, K., Kitagawa, D., Watanabe, T., Momose, H., Ohata, S., Tanemura, S. et al. (2004) Stress induces mitochondria-mediated apoptosis independent of SAPK/JNK activation in embryonic stem cells. J. Biol. Chem. **279**, 1621–1626

10 Dhanasekaran, D. N., Kashef, K., Lee, C. M., Xu, H. and Reddy, E. P. (2007) Scaffold proteins of MAP-kinase modules. Oncogene **26**, 3185–3202

11 Nishina, H., Nakagawa, K., Azuma, N. and Katada, T. (2003) Activation mechanism and physiological roles of stress-activated protein kinase/c-Jun NH_2-terminal kinase in mammalian cells. J. Biol. Regul. Homeost. Agents **17**, 295–302

12 Marti, A., Luo, Z., Cunningham, C., Ohta, Y., Hartwig, J., Stossel, T. P., Kyriakis, J. M. and Avruch, J. (1997) Actin-binding protein-280 binds the stress-activated protein kinase (SAPK) activator SEK-1 and is required for tumor necrosis factor-α activation of SAPK in melanoma cells. J. Biol. Chem. **272**, 2620–2628

13 Tournier, C., Whitmarsh, A. J., Cavanagh, J., Barrett, T. and Davis, R. J. (1999) The MKK7 gene encodes a group of c-Jun NH_2-terminal kinase kinases. Mol. Cell. Biol. **19**, 1569–1581

14 Kitagawa, D., Kajiho, H., Negishi, T., Ura, S., Watanabe, T., Wada, T., Ichijo, H., Katada, T. and Nishina, H. (2006) Release of RASSF1C from the nucleus by Daxx degradation links DNA damage and SAPK/JNK activation. EMBO J. **25**, 3286–3297

15 Cunningham, C. C., Gorlin, J. B., Kwiatkowski, D. J., Hartwig, J. H., Janmey, P. A., Byers, H. R. and Stossel, T. P. (1992) Actin-binding protein requirement for cortical stability and efficient locomotion. Science **255**, 325–327

16 Ohta, Y., Suzuki, N., Nakamura, S., Hartwig, J. H. and Stossel, T. P. (1999) The small GTPase RalA targets filamin to induce filopodia. Proc. Natl. Acad. Sci. U.S.A. **96**, 2122–2128

17 Leonardi, A., Ellinger-Ziegelbauer, H., Franzoso, G., Brown, K. and Siebenlist, U. (2000) Physical and functional interaction of filamin (actin-binding protein-280) and tumor necrosis factor receptor-associated factor 2. J. Biol. Chem. **275**, 271–278

18 Huang, C., Rajfur, Z., Borchers, C., Schaller, M. D. and Jacobson, K. (2003) JNK phosphorylates paxillin and regulates cell migration. Nature **424**, 219–223

19 Otto, I. M., Raabe, T., Rennefahrt, U. E., Bork, P., Rapp, U. R. and Kerkhoff, E. (2000) The p150-Spir protein provides a link between c-Jun N-terminal kinase function and actin reorganization. Curr. Biol. **10**, 345–348

20 Nomachi, A., Nishita, M., Inaba, D., Enomoto, M., Hamasaki, M. and Minami, Y. (2008) Receptor tyrosine kinase Ror2 mediates Wnt5a-induced polarized cell migration by activating c-Jun N-terminal kinase via actin-binding protein filamin A. J. Biol. Chem. **283**, 27973–27981

21 Jeon, Y. J., Choi, J. S., Lee, J. Y., Yu, K. R., Ka, S. H., Cho, Y., Choi, E-J., Baek, S. H., Seol, J. H., Park, D. et al. (2008) Filamin B serves as a molecular scaffold for type I interferon-induced c-Jun NH_2-terminal kinase signaling pathway. Mol. Biol. Cell **19**, 5116–5130

22 Jeon, Y. J., Choi, J. S., Lee, J. Y., Yu, K. R., Kim, S. M., Ka, S. H., Oh, K. H., Kim, K. I., Zhang, D-E., Bang, O.S. and Chung, C.H. (2009) ISG15 modification of filamin B negatively regulates the type I interferon-induced JNK signalling pathway. EMBO Rep. **10**, 374–380

Received 6 July 2009/5 February 2010; accepted 15 February 2010
Published as BJ Immediate Publication 15 February 2010, doi:10.1042/BJ20091011

STEM CELLS AND DEVELOPMENT
Volume 19, Number 11, 2010

DOI: 10.1089/scd.2010.0066

p38 Mitogen-Activated Protein Kinase Controls a Switch Between Cardiomyocyte and Neuronal Commitment of Murine Embryonic Stem Cells by Activating Myocyte Enhancer Factor 2C-Dependent Bone Morphogenetic Protein 2 Transcription

Jinzhan Wu,[1,2,*] Junko Kubota,[2,*] Jun Hirayama,[3,*] Yoko Nagai,[1,2] Sachiko Nishina,[4] Tadashi Yokoi,[1,4] Yoichi Asaoka,[1] Jungwon Seo,[1,2] Nao Shimizu,[1,2] Hiroaki Kajiho,[2] Takashi Watanabe,[5] Noriyuki Azuma,[4] Toshiaki Katada,[2] and Hiroshi Nishina[1]

Many studies have shown that it is possible to use culture conditions to direct the differentiation of murine embryonic stem (ES) cells into a variety of cell types, including cardiomyocytes and neurons. However, the molecular mechanisms that control lineage commitment decisions by ES cells remain poorly understood. In this study, we investigated the role of the 3 major mitogen-activated protein kinases (MAPKs: extracellular signal-regulated kinase, c-Jun N-terminal kinase, and p38) in ES cell lineage commitment and showed that the p38 MAPK-specific inhibitor SB203580 blocks the spontaneous differentiation of ES cells into cardiomyocytes and instead induces the differentiation of these ES cells into neurons. Robust p38 MAPK activity between embryoid body culture days 3 and 4 is crucial for cardiomyogenesis of ES cells, and specific inhibition of p38 MAPK activity at this time results in ES cell differentiation into neurons rather than cardiomyocytes. At the molecular level, inhibition of p38 MAPK activity suppresses the expression of *bmp-2* mRNA, whereas treatment of ES cells with bone morphogenetic protein 2 (BMP-2) inhibits the neurogenesis induced by SB203580. Further, luciferase reporter assays and chromatin immunoprecipitation experiments showed that BMP-2 expression in ES cells is regulated directly by the transcription factor myocyte enhancer factor 2C, a well-known substrate of p38 MAPK. Our findings reveal the molecular mechanism by which p38 MAPK activity in ES cells drives their commitment to differentiate preferentially into cardiomyocytes, and the conditions under which these same cells might develop into neurons.

Introduction

MURINE EMBRYONIC STEM (MES) CELLS are stem cells derived from the inner cell mass of embryonic day 3.5 (E3.5) blastocysts [1,2]. In the presence of leukemia inhibitory factor (LIF), mES cells can be maintained in an undifferentiated state *in vitro* and retain their potential for unlimited proliferation [3,4]. When LIF is removed from the culture and appropriate induction conditions are applied, ES cells can be directed to differentiate *in vitro* into a variety of cell lineages, including cardiomyocytes and neurons [5]. In humans, therapeutic transplantation of ES cells or their derivatives has been proposed as a potential treatment for various diseases. However, the molecular mechanisms governing the commitment of ES cells to specific cell lineages remain poorly understood. Elucidation of these mechanisms would greatly improve the efficiency of applied ES cell differentiation approaches.

The extracellular signal-regulated kinases (ERKs), c-Jun N-terminal kinases (JNKs), and p38 kinases are the 3 major groups of mitogen-activated protein kinases (MAPKs) found in mammals [6,7]. ERK1 and ERK2 are widely expressed and

[1]Department of Developmental and Regenerative Biology, Medical Research Institute, [3]Medical Top Track Program, Medical Research Institute, Tokyo Medical and Dental University, Tokyo, Japan.
[2]Department of Physiological Chemistry, Graduate School of Pharmaceutical Sciences, University of Tokyo, Tokyo, Japan.
[4]Department of Ophthalmology, National Center for Child Health and Development, Tokyo, Japan.
[5]Department of Laboratory Medicine, Kyorin University School of Medicine, Tokyo, Japan.
*These authors contributed equally to this work.

involved in the regulation of meiosis, mitosis, and post-mitotic functions in differentiated cells. In contrast, the JNK enzymes are important for controlling cell survival and apoptosis. The p38 kinases, which regulate the expression of many cytokines, were first identified in lipopolysaccharide-stimulated murine macrophages and in a screen for drugs able to inhibit tumor necrosis factor-α-mediated inflammatory responses in human monocytes [8,9]. Immune system cells that encounter inflammatory cytokines respond by activating p38, and this MAPK then supports the activation of immune responses. Four different p38 isoforms, p38α, p38β, p38γ, and p38δ, have been identified in mammalian cells [10]. The p38α and p38β isoforms are expressed in murine heart, whereas p38γ and p38δ are expressed at low levels in this organ. Deletion of the p38α gene in mice leads to early embryonic lethality between E11.5 and E12.5 [11,12]. On the other hand, p38β gene-targeted mice are viable and exhibit no apparent health problems [13]. It has been demonstrated that p38α associates with the transcription factor myocyte enhancer factor 2C (MEF2C), which is a member of the MADS-box family [14]. Phosphorylation of MEF2C by p38 stimulates MEF2C's ability to activate transcription of its target genes. In mammals, there are 4 MEF2 family genes, namely MEF2A, MEF2B, MEF2C, and MEF2D, which form homo- and heterodimers and bind to the DNA consensus sequence $CTA(A/T)_4TA(G/A)$ [15,16]. This sequence is found in the promoter regions of numerous muscle-specific genes, as well as in genes induced by growth factors or stress. A major role of the MEF2C protein is to regulate muscle-specific gene expressions. For example, loss-of-function mutations in myocyte enhancer factor 2C (*mef2c*) severely disrupt early cardiogenesis [17] and vascular development [18], suggesting that MEF2C may be critical for cardiomyogenesis by ES cells. However, the role of MEF2C in neural commitment is unknown.

Several extracellular signaling pathways are important for both embryonic and tissue stem cell determination, including pathways involving the Wnt proteins and the bone morphogenetic proteins (BMPs) [19,20]. However, a detailed understanding of the molecular mechanisms underlying the regulation of stem cell fate by these extracellular factors is lacking. BMPs are members of the transforming growth factor-β (TGF-β) superfamily and are known to function in the development and regulation of a wide range of biological systems. These extracellular ligands were originally isolated as components of bone extracts that induced ectopic cartilage and bone formation when implanted in muscle [21]. However, BMPs have since been demonstrated to function in multiple developmental processes, including dorsoventral patterning within the neural tube, the induction of mesoderm during gastrulation, and hematopoiesis [22]. As might be expected from these complex *in vivo* functions, BMPs also play key roles in regulating fate choices during tissue stem cell differentiation. For example, BMPs direct mesenchymal stem cells to differentiate into chondrogenic and osteogenic cell lineages [20]. BMPs have also been shown to regulate fate choices in neural crest stem cells [23].

In this study, we demonstrate that p38 MAPK controls an ES cell fate choice between cardiomyocytes and neurons. Further, our results show that this choice is mediated by the action of BMP-2, whose transcription is directly regulated by the p38 MAPK substrate MEF2C.

Materials and Methods

Cell culture and ES cell differentiation

Feeder cell-independent E14K ES cells were maintained on a gelatin-coated dish with Dulbecco's modified Eagle's medium (Gibco) containing 15% fetal bovine serum (FBS) (HyClone, Lot No. AMC15813), 0.1% 2-mercaptoethanol (Sigma), and 1000 U/mL LIF (propagation medium), as described previously [24–27]. To induce cardiomyocyte differentiation, LIF was removed from the propagation medium and 3×10^3 ES cells suspended in a 25 μL hanging drop. The drop was placed on the lid of an inverted bacterial Petri dish so that the cells would eventually attach and form embryoid bodies (EBs). After 2 days (on day 3), the EBs were collected and transferred into a bacterial Petri dish. After 4 days of suspension culture (on day 7), the EBs were plated on a gelatin-coated tissue culture dish. Areas of tissue showing a spontaneous "heartbeat" were readily detected on day 12.

For MAPK inhibition experiments, SB203580 (10 μM; Calbiochem), U0126 (10 μM; Promega), SP600125 (5 μM; Biomol), or wortmannin (1 μM; Wako) was added to EB cultures on day 1. For BMP-2 experiments, recombinant human BMP-2 (3 ng/mL; R&D Systems) or BMP-2 antagonist Noggin (100 ng/mL; R&D Systems) was added to EB culture on days 4–6.

Microscopic analysis of cardiomyocytes and neurons

Individual EBs, prepared as described earlier, were plated onto gelatin-coated 96-well tissue culture plates on day 7. The numbers of spontaneously beating EBs and EBs with neurite outgrowths were counted on day 12 under a phase-contrast microscope. Data were expressed as the percentage of the total number of EBs plated.

Immunofluorescence and immunohistochemistry

Immunofluorescence staining was performed as described previously [26]. For immunohistochemistry (IHC), EBs were fixed in 4% paraformaldehyde (PFA)–phosphate-buffered saline (PBS) for 2 h at 4°C, washed sequentially with PBS, 10% sucrose/PBS/0.02% NaN_3, 15% sucrose/PBS/0.02% NaN_3, and 20% sucrose/PBS/0.02% NaN_3, and embedded in OCT compound (Tissue Tek) with liquid nitrogen. Frozen sections were cut at 10 μm and placed on 3-aminopropyltriethoxy-silane (APES)-coated slides. After air drying, sections were fixed in acetone at room temperature for 10 min, rinsed in PBS, and incubated in 0.3% H_2O_2/PBS for 30 min to block endogenous peroxidases. After preincubation with blocking solution (5% bovine serum albumin/PBS/0.1% Tween 20) for 1 h, slides were incubated overnight at 4°C with a 1:800 dilution of anti-α-actinin antibody (cardiac specific) or a 1:500 dilution of anti-TuJ-1 (neuron-specific class III β-tublin) antibody. After 3×5 min washes in PBS/0.05% Tween 20 (PBST), sections were incubated with biotinylated secondary antibodies (Vectastain Elite ABC Kit) for 2 h. Slides were washed again in PBST and incubated for 1 h with Vectastain Elite ABC Reagent. Following a last wash in PBST, sections were incubated in 3,3'-Diaminobenzidine (DAB) solution (200 μg/mL DAB, 0.015% H_2O_2/PBS) until a color change was observed (2–10 min), and slides were rinsed in PBS. Finally, sections were counterstained with hematoxylin at room temperature for 1 min, washed, dehydrated, mounted, and inspected using a phase-contrast microscope.

Reverse transcriptase–polymerase chain reaction analysis

ES cells, EBs, or mouse organs (brain, heart, liver) from E12.5 mouse embryos were lysed with Trizol reagent (Invitrogen), and first-strand cDNA was synthesized using SuperScript III RNase H–reverse transcriptase (Invitrogen). The primers used in polymerase chain reactions (PCRs) are shown in Supplementary Table S1 (available online at www.liebertonline.com/scd).

Western blotting analysis

EBs were lysed and fractionated by sodium dodecyl sulfate–polyacrylamide gel electrophoresis and immunoblotted with antibody against total p38 (C-20; Santa Cruz Biotechnology) or phospho-p38 MAPK (Thr180/Tyr182) (Cell Signaling Technologies, No. 9211). Horseradish peroxidase-conjugated goat anti-rabbit IgG was used as the secondary antibody. Bands were observed using SuperSignal West Pico Chemiluminescent Substrate (Pierce) for total p38, or SuperSignal West Femto maximum sensitivity substrate (Pierce) for phospho-p38, as described previously [28].

Luciferase reporter assays

A proximal promoter region (−1703/−1) of mouse *bmp-2* containing the MEF2 binding site was amplified by PCR using the upstream primer 5′-CGACGCGTCTGTCCA GAGGCATCCATTT-3′ and the downstream primer 5′-CGCTCGAGAACACCTCCCCCTCGGA-3′. The sequence was confirmed and cloned into the pTAL-Luc reporter vector (pTAL-BMP-2-Luc). HeLa cells were cotransfected with pTAL-BMP-2-Luc and pcDNA3-Mef2c expressing MEF2C using FuGENE 6 transfection reagent (Roche Molecular Biochemicals). Luciferase activity was assayed at 24 h after transfection using the dual-luciferase reporter assay system (Promega) following the manufacturer's protocols.

Chromatin immunoprecipitation

Chromatin immunoprecipitation (ChIP) assays were performed according to published protocols from Cosmo Bio (http://www.cosmobio.co.jp) with minor modifications. EBs were fixed by adding 1% formaldehyde to the culture medium for 10 min at 25°C. Anti-MEF2C antibody (E-17; Santa Cruz Biotechnology) and control anti-actin IgG (I-19; Santa Cruz Biotechnology) were used to immunoprecipitate chromatin. The sequences of the ChIP primers were 5′-TCTG GAGTAGGTGGGTGTGG-3′ and 5′-CATGTGAGGGGACA ATGAGA-3′ for *bmp-2*; 5′-GGTGGGGAGAGAGCAGTTC-3′ and 5′-GTGAGATGCGTGATCCCTCT-3′ for *mef2c*; and 5′-GGAAAGGGGGTGTTGTTCTT-3′ and 5′-CCCTGACCATC ACCCTTCTA-3′ for the negative control gene bromo adjacent homology domain containing 1 (*bahd1*).

Results

The p38-specific inhibitor SB203580 and the ERK-specific inhibitor U0126 block spontaneous ES cell cardiomyogenesis

To identify the kinases most important for ES cell lineage commitment, we treated EBs with the ERK-specific inhibitor U0126, the JNK-specific inhibitor SP600125, the p38 MAPK-specific inhibitor SB203580, or the PI3K-specific inhibitor wortmannin. The inhibitors were applied to the EB cultures for the interval spanning days 1–6 during the EB differentiation process. We found that only the ERK-specific inhibitor U0126 and the p38 MAPK-specific inhibitor SB203580 blocked spontaneous cardiomyocyte differentiation, and that this block was so profound that fewer than 5% of EBs contained beating foci at day 12 (Fig. 1A). In contrast, more than 90% of untreated control EBs contained beating areas, which were confirmed as cardiac in commitment by phenotypic testing. Intriguingly, more than 90% of SB203580-treated EBs (but not U0126-treated EBs) continued to exhibit prominent outgrowths even though cardiomyogenesis was inhibited (Fig. 1B). These outgrowths stained positively with an anti-βIII-tubulin antibody specific for neurons, in contrast to the negative staining displayed by untreated EBs and EBs treated with U0126 (Fig. 1C, D). These results demonstrate that SB203580 blocks cardiomyocyte differentiation and induces neural differentiation, but that neural differentiation does not depend solely on the inhibition of cardiomyogenesis.

SB203580-mediated inhibition of p38 MAPK blocks cardiomyogenesis and commits ES cell differentiation to the neuronal lineage

To confirm that SB203580 had a switch effect on cardiac versus neural ES cell differentiation, frozen sections from EBs that had been untreated or treated with SB203580 between days 1 and 6 were subjected to IHC at day 12. SB203580-treated EBs did not stain positively with an antibody recognizing the cardiac-specific marker α-actinin, but did stain with an anti-TuJ-1 antibody specific for neurons (Fig. 2A). RT-PCR analysis of a set of embryonic genes revealed that SB203580 treatment completely inhibited the mRNA expression of the cardiac-associated *mef2c*, α-cardiac myosin heavy chain (*mhc*), and myosin light chain 2v (*mlc2v*) genes (Fig. 2B), but induced significant increases in the mRNA levels of the neuronal lineage genes *nestin*, hairy and enhancer of split 5 (*hes5*), mammalian achate schute homolog 1 (*mash1*), mouse atherosclerosis 3 (*math3*), and microtubule-associated protein 2 (*map2*) (Fig. 2C).

p38 MAPK activity between days 3 and 4 serves as a switch determining cardiac or neural commitment of ES cells

To define the role of p38 MAPK in ES cell commitment, we used immunoblotting to measure p38 MAPK activation during the earliest stages of ES cell differentiation. At day 0, when ES cells were cultured as a monolayer, no detectable phospho-p38 MAPK (activated enzyme) could be detected in whole cell lysates. However, after EB formation at day 2, high levels of phospho-p38 MAPK spontaneously appeared and were maintained until day 6; total p38 MAPK protein levels were not affected (Fig. 3A). To determine at what time point p38 MAPK acts during ES cell differentiation, we treated EBs with SB203580 for specific time intervals. As shown in Fig. 3B, when EBs were exposed to SB203580 between days 3 and 4, neuron differentiation was promoted at the expense of cardiomyocyte differentiation, an effect replicated by SB203580 treatment from day 0 to 6. In contrast, exposure to SB203580 for other intervals did not interfere

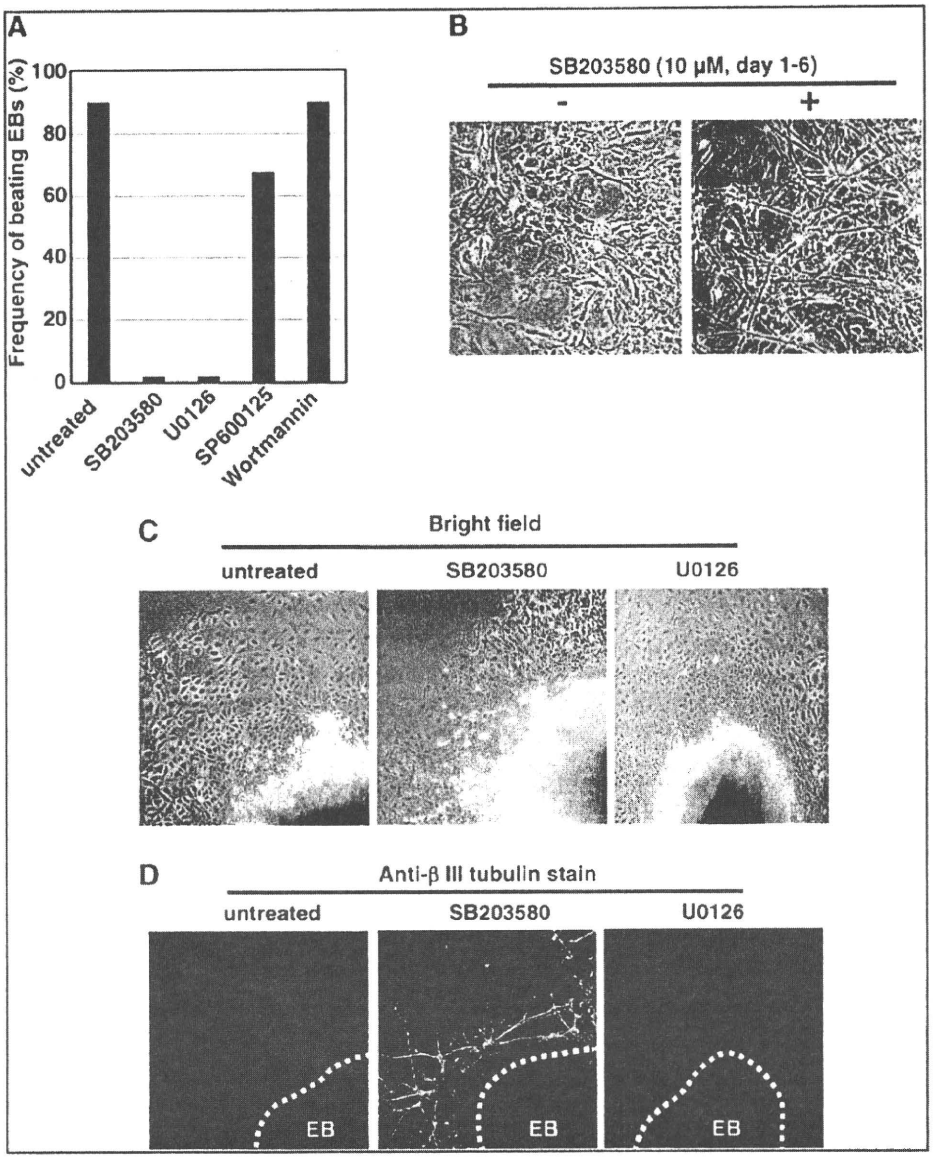

FIG. 1. Effects of specific mitogen-activated protein kinase inhibitors on embryonic stem (ES) cell differentiation. **(A)** Specific involvement of extracellular signal-regulated kinase (ERK) and p38 in cardiac differentiation. Embryoid bodies (EBs) were left untreated or treated with the p38-specific inhibitor SB203580 (10 μM), the ERK-specific inhibitor U0126 (10 μM), the c-Jun N-terminal kinase-specific inhibitor SP600125 (5 μM), or the PI3K-specific inhibitor wortmannin (1 μM) for the EB differentiation for the whole 6 days. Cardiomyocyte differentiation was determined by counting the number of EBs containing beating foci at day 12. Results are expressed as the mean percentage of total EBs plated. **(B)** Neurite outgrowths in the presence of SB203580. EBs were left untreated (−) or treated with 10 μM SB203580 (+) for days 1 – 6. Outgrowths were detected by photomicrography of EBs at day 12. **(C, D)** Neuronal differentiation. EBs were treated with SB203580 (p38) or U0126 (ERK) as in (A). On day 12, EB outgrowths were immunostained with anti-β-tubulin antibody specific for neuronal lineage cells and subjected to photomicrography. Bright field images by phase-contrast microscopy are shown. Dotted line: physical edge of EB in culture.

with spontaneous cardiomyocyte generation and did not induce neurogenesis. To examine dose-dependent effects of SB203580 on ES cell differentiation, we treated EBs with various concentrations of SB203580. As shown in Fig. 3C, when EBs were exposed to SB203580 between days 3 and 6, neuron differentiation was promoted at the expense of cardiomyocyte differentiation in a dose-dependent manner. RT-PCR analysis confirmed that the expression of the neuronal markers *hes5* and *map2* was induced only when SB203580 was applied to EBs between days 3 and 4, or between days 1 and 6, whereas expression of the cardiomyocyte-specific genes *mhc* and *mlc2v* was strongly decreased at these times

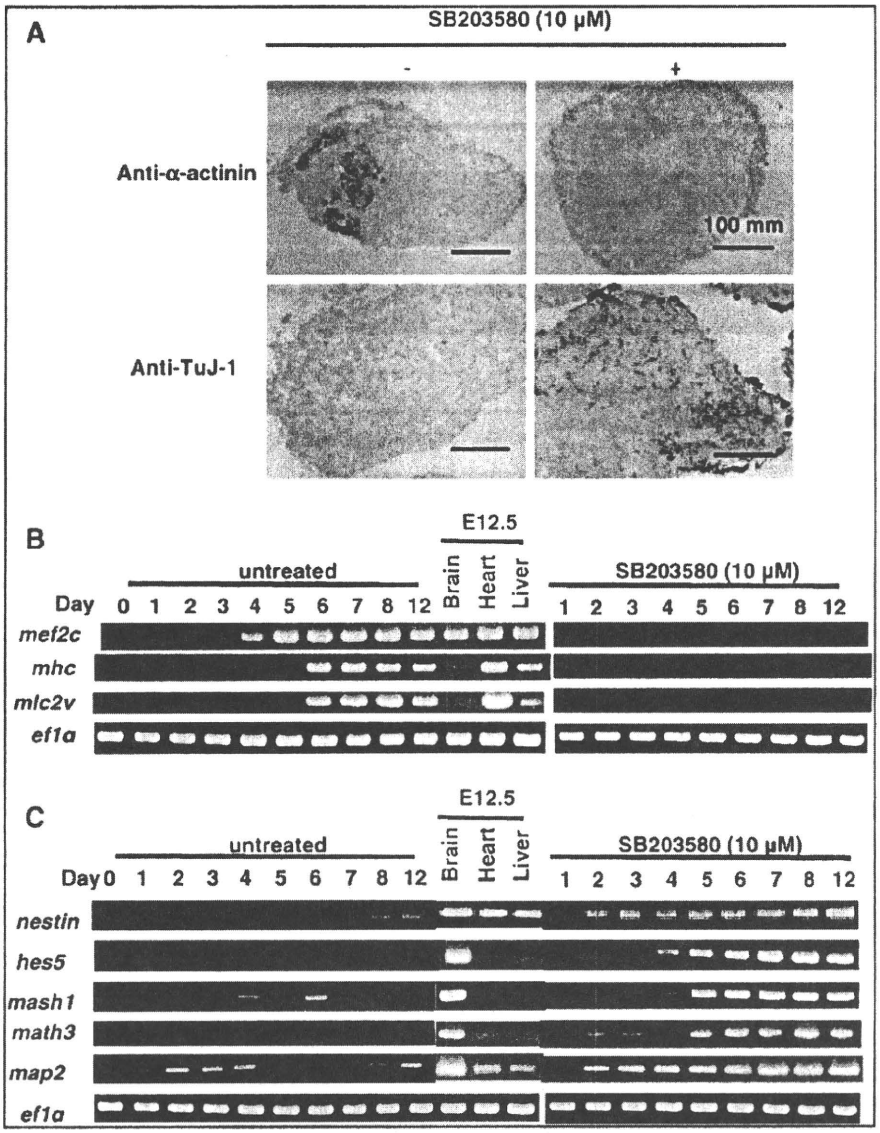

FIG. 2. SB203580-mediated inhibition of p38 mitogen-activated protein kinase blocks cardiomyogenesis and commits ES cells to the neuronal lineage. **(A)** Immunostaining. Embryoid bodies (EBs) were left untreated or treated with 10 μM SB203580 for days 1–6. EBs were harvested on day 7 and frozen sections were immunostained with anti-α-actinin antibody specific for cardiomyocytes or anti-TuJ-1 antibody specific for neurons. **(B)** Reduced cardiac gene expression. EBs were left untreated or treated with 10 μM SB203580 from day 1 until the indicated day, and extracts were analyzed by reverse transcriptase–polymerase chain reaction (RT–PCR) to detect mRNA expression of the cardiac-specific genes myocyte enhancer factor 2C (*mef2c*), α-cardiac myosin heavy chain (*mhc*), and myosin light chain 2v (*mlc2v*). Elongation factor 1α (*ef1a*) was used as the loading control. E12.5 brain, heart, and liver served as positive controls for the expression of various mRNAs. **(C)** Increased neuronal gene expression. EBs were left untreated or treated with 10 μM SB203580 from day 0 until the indicated day, and extracts were analyzed by RT-PCR to detect mRNA expression of the neuron-specific genes *nestin*, hairy and enhancer of split 5 (*hes5*), mammalian achate schute homolog 1 (*mash1*), *math3*, and microtubule-associated protein 2 (*map2*). Controls used were as same as for (B).

(Fig. 3C). These results clearly demonstrate that p38 MAPK activity spanning days 3 and 4 is critical for the cardiac commitment of ES cells, and that interference with this p38 MAPK activity drives neurogenesis instead.

p38 MAPK controls the expression of BMP-2 during ES cell differentiation

To elucidate the molecular mechanism by which p38 MAPK governs cell fate choices in ES cells, we sought to identify relevant downstream targets of this kinase. Because p38 MAPK activity spanning days 3 and 4 was found to be crucial for lineage commitment, we investigated whether the mRNA expression of genes known to be involved in ES cell fate decisions was affected by treating the EBs with SB203580 for this interval. Notably, RT-PCR analysis showed that the expression of the *bmp*-2 mRNA, which normally commences on day 4, was decreased by SB203580 exposure compared with the untreated control (Fig. 4A). This effect was specific to *bmp*-2 as none of the other genes examined showed any SB203580-induced difference in mRNA expression. Further analysis confirmed that *bmp*-2 mRNA was first induced on day 4, and that SB203580 strongly repressed (but did not extinguish) this induction (Fig. 4B). On the other hand, U0126 did not repress the induction of *bmp*-2 mRNA (Fig. 4C). These results indicate that p38 MAPK but not ERK regulates the induction of *bmp*-2 mRNA in this ES cell differentiation.

BMP-2 inhibits SB203580-induced neuronal differentiation

To determine whether it was the downregulation of BMP-2 in SB203580-treated EBs that committed them to neurogenesis, we treated EBs that had been exposed to SB203580 on days 3–6 with recombinant human BMP-2 (rhBMP-2) on

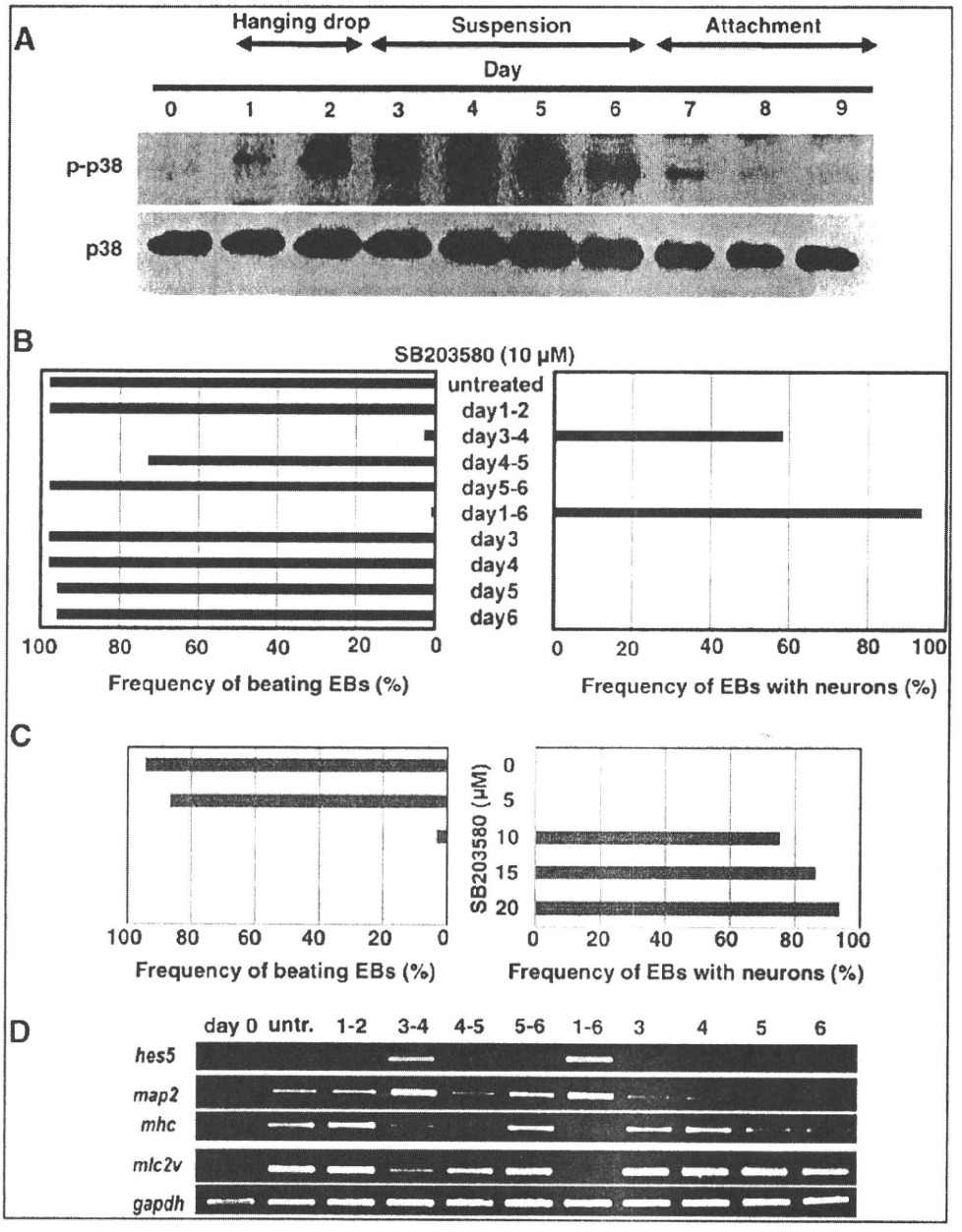

FIG. 3. p38 mitogen-activated protein kinase (MAPK) activity spanning days 3 and 4 serves as a switch determining cardiac or neuronal commitment of ES cells. **(A)** Spontaneous p38 MAPK activation spans days 2–6. Untreated embryoid bodies (EBs) were cultured from day 1 to 9, and whole cell extracts were subjected to Western blotting to detect phospho-p38 MAPK (p-p38, active enzyme) and total p38 MAPK protein (p38). **(B)** SB203580 treatment spanning days 3–4 induces switching. EBs were left untreated or treated with 10 μM SB203580 for the indicated time periods. On day 12, cardiomyocyte or neuronal differentiation was determined by counting numbers of EBs containing beating foci or showing neurite outgrowths. Results are expressed as the percentage of total EBs plated that showed cardiac or neuronal features. **(C)** Effects of SB203580 concentration on ES cell differentiation. EBs were left untreated or treated with the indicated concentrations of SB203580 from day 3 to 6. On day 12, cardiomyocyte or neuronal differentiation was determined as for (B). **(D)** Decreased cardiac but increased neuronal mRNAs. Extracts of the EBs in (B) were analyzed by reverse transcriptase (RT)–polymerase chain reaction to detect mRNA expression of cardiac-specific [α-cardiac myosin heavy chain (*mhc*), myosin light chain 2v (*mlc2v*)] and neuron-specific [hairy and enhancer of split 5 (*hes5*), microtubule-associated protein 2 (*map2*)] genes. Glyceraldehyde-3-phosphate dehydrogenase (*gapdh*), loading control; untr., untreated.

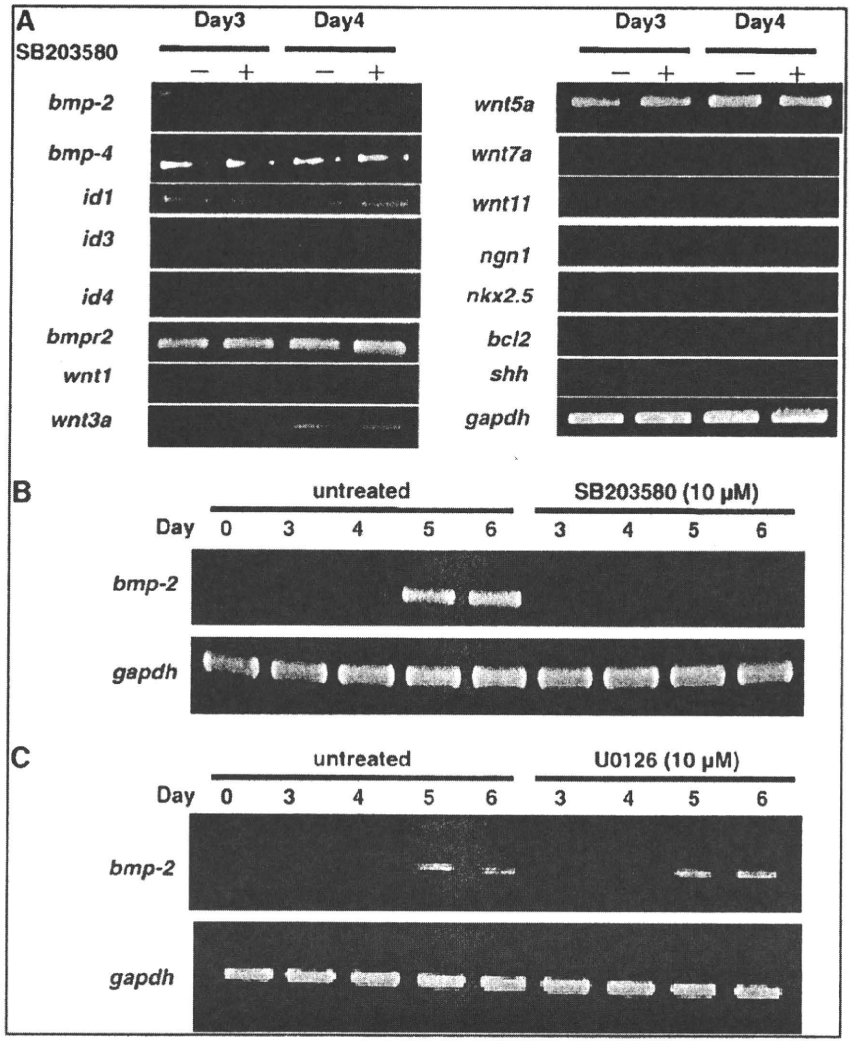

FIG. 4. p38 mitogen-activated protein kinase (MAPK) controls the expression of bone morphogenetic protein 2 (BMP-2) during ES cell differentiation. **(A)** SB203580 decreases *bmp-2* mRNA. Embryoid bodies (EBs) were left untreated or treated for days 3–4 with 10 μM SB203580. Extracts were analyzed by reverse transcriptase–polymerase chain reaction (RT–PCR) to evaluate transcript levels of the indicated cell fate-associated genes *bmp-2*, *bmp-4*, inhibitor of DNA binding 1 (*id1*), *id3*, *id4*, *bmp* receptor type II (*bmpr2*), wingless-type MMTV integration site family, member 1 (*wnt1*), *wnt3a*, *wnt5a*, *wnt7a*, *wnt11*, neurogenin 1 (*ngn1*), NK2 transcription factor related, locus 5 (*nkx2.5*), B-cell leukemia/lymphoma 2 (*bcl2*), and sonic hedgehog (*shh*). **(B, C)** p38 MAPK-mediated induction of *bmp-2* commences on day 4. EBs were left untreated or treated with 10 μM SB203580 or 10 μM U0126 on days 3–6 and *bmp-2* mRNA levels were determined by RT-PCR. Glyceraldehyde-3-phosphate dehydrogenase (gapdh) was used as the loading control.

days 4–6. As predicted, the neuronal differentiation induced by SB203580 treatment was dramatically repressed by rhBMP-2 treatment (Fig. 5A). A quantitative analysis showed that SB203580 treatment on days 3–6 induced nearly 80% of EBs to generate neuronal lineage cells, whereas the addition of rhBMP-2 on days 4–6 reduced this rate to fewer than 5% of EBs (Fig. 5B). Consistent with the microscopic analysis, RT-PCR confirmed that rhBMP-2 strongly inhibited SB203580-induced expression of the neuron-specific gene *map2* (Fig. 5C, top row). In contrast, expression levels of the cardiomyocyte-specific genes *mhc* and *mlc2v* in SB203580-treated EBs were not improved by the addition of rhBMP-2 (Fig. 5C, middle row).

The BMP-2 antagonist Noggin blocks cardiomyogenesis and induces neural differentiation

On the basis of the above results, we postulated that vigorous interference with endogenous BMP-2 function might prevent the differentiation of ES cells into cardiomyocytes and induce neurogenesis. To test this hypothesis, we treated EBs with the BMP-2 antagonist Noggin on days 4–6. Like SB203580 treatment, Noggin treatment of EBs at this time dramatically blocked cardiomyogenesis and promoted neuronal differentiation (Fig. 6A). A quantitative analysis showed that more than 60% of EBs treated with 100 ng/mL Noggin on days 4–6 differentiated into neurons, a rate similar to the 75% of EBs induced to undergo neurogenesis by SB203580 treatment on days 3–6 (Fig. 6B). Moreover, RT-PCR analysis confirmed that Noggin treatment strongly induced the expression of the neuronal gene *map2* and repressed expression of the cardiac gene *mhc* (Fig. 6C). Taken together, these results indicate that p38 MAPK controls ES cell lineage commitment (at least with respect to cardiomyocyte vs. neuron differentiation) by regulating the expression of BMP-2.

BMP-2 is a direct transcriptional target of MEF2C

The above experiments revealed that treatment of EBs with SB203580 resulted in a dramatic decrease in the mRNA expression of the transcription factor MEF2C, a well-known substrate of p38 MAPK (refer to Fig. 2B). We therefore compared the expression patterns of *mef2c* and *bmp-2* during

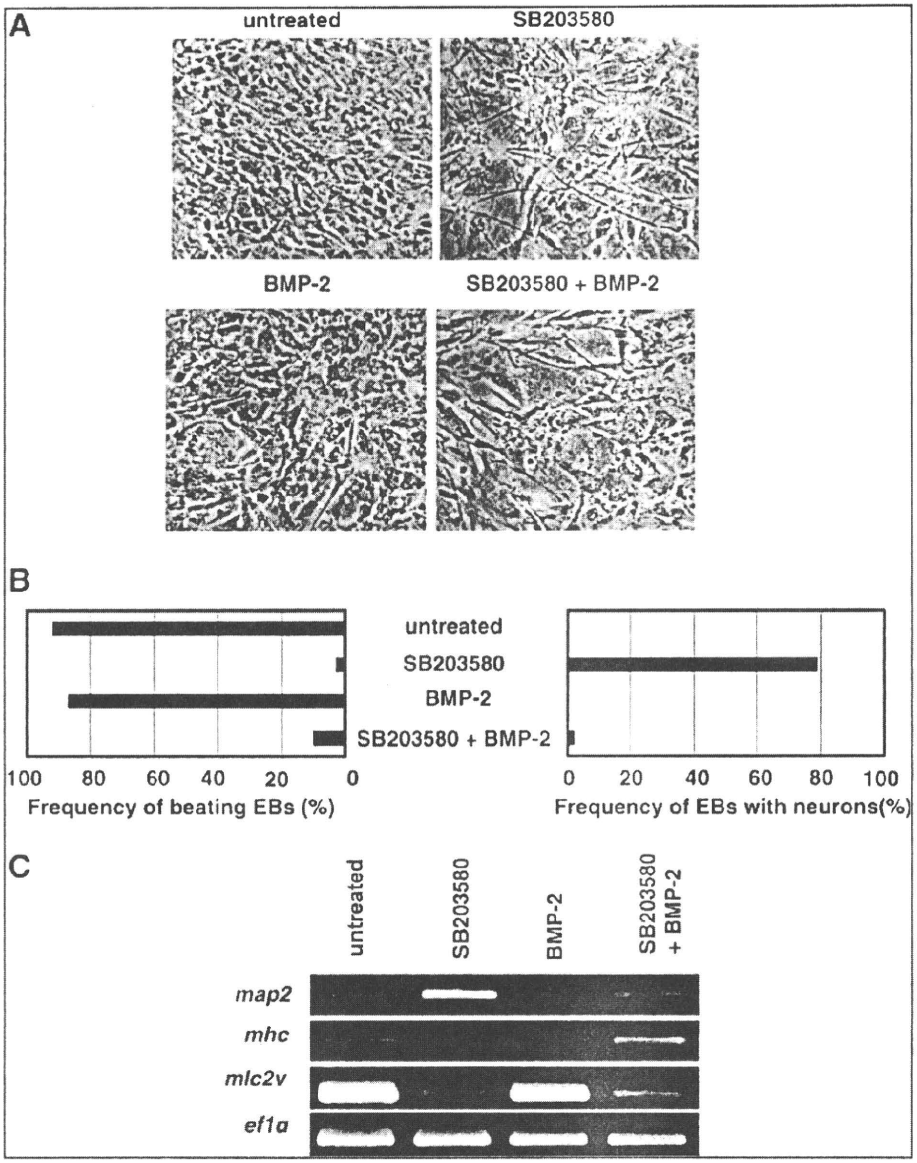

FIG. 5. Bone morphogenetic protein 2 (BMP-2) inhibits SB203580-induced neuronal differentiation. Embryoid bodies (EBs) were left untreated or treated with 3 ng/mL recombinant human BMP-2 on days 4–6 in the presence or absence of 10 μM SB203580 on days 3–6. **(A)** Outgrowth suppression. Photomicrographs of EBs at day 12 are shown. **(B)** Reduced frequency of EBs with neurons. EBs containing beating foci or neurite outgrowths were counted on day 12. Results are expressed as a percentage of EBs plated. **(C)** Increased cardiac but decreased neuronal mRNAs. Extracts of the EBs in (A) were analyzed by reverse transcriptase (RT)–polymerase chain reaction to determine mRNA levels of the indicated cardiac-specific [α-cardiac myosin heavy chain (*mhc*), myosin light chain 2v (*mlc2v*)] and neuronal [microtubule-associated protein 2 (*map2*)] genes. Elongation factor 1α (ef1α) was used as the loading control.

SB203580-induced neuronal differentiation and found that they were strikingly similar (Fig. 7A). Once activated by p38 MAPK-mediated phosphorylation, MEF2C activates the transcription of many cardiac-specific genes. Our observations suggested that p38 MAPK might induce BMP-2-regulated cardiomyogenesis by EBs via direct regulation of MEF2C. Importantly, a highly conserved consensus binding site for MEF2 has been identified in both the mouse and human proximal BMP-2 promoters. To test whether MEF2C could directly regulate BMP-2 transcription, we first carried out reporter assays in HeLa cells in which luciferase was placed under the control of a proximal region (−1703/−1 bp) of the mouse *bmp-2* promoter; this region contains the MEF2-binding site. HeLa cells engineered to overexpress MEF2C showed a 3-fold increase in luciferase activity, whereas SB203580 treatment repressed this transactivation (Fig. 7B).

To determine whether MEF2C could physically bind to the BMP2 promoter region, we carried out ChIP analyses of day

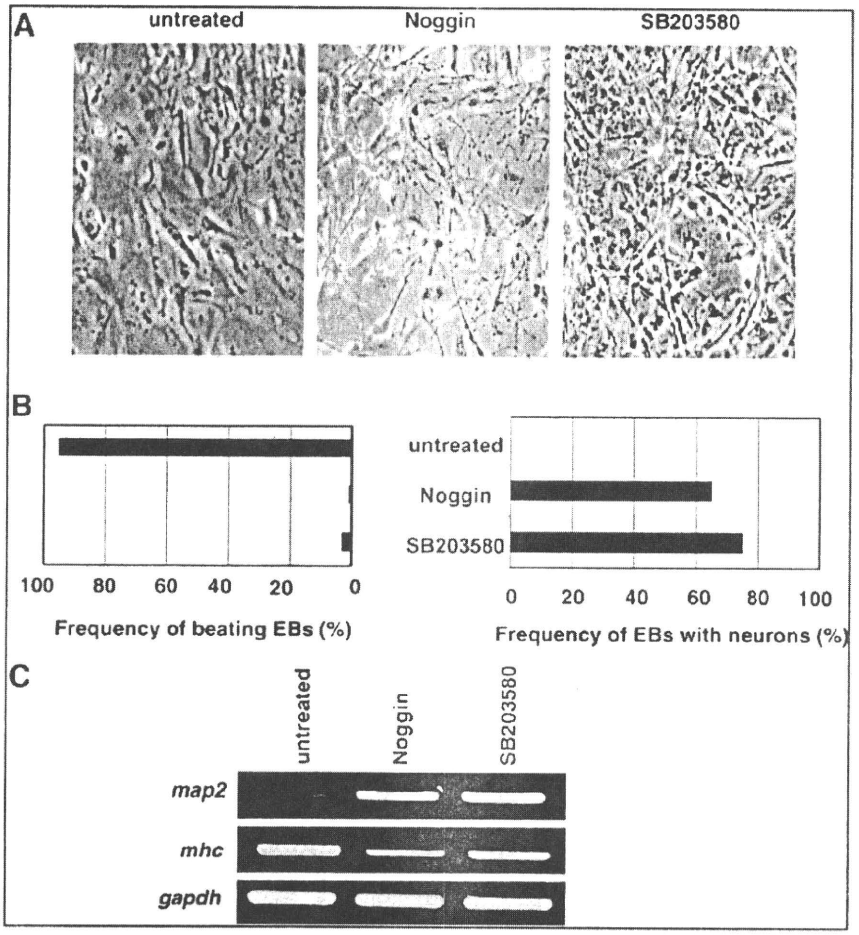

FIG. 6. The bone morphogenetic protein 2 antagonist Noggin blocks cardiomyogenesis and induces neuronal differentiation. Embryoid bodies (EBs) were left untreated or treated with 100 ng/mL Noggin on days 4–6, or with 10 μM SB203580 on days 3–6. **(A)** Outgrowth promotion. Photomicrographs of EBs at day 12 are shown. **(B)** Increased frequency of EBs with neurons. EBs containing beating foci or neurite outgrowths were counted on day 12. Results are expressed as a percentage of EBs plated. **(C)** Increased neuronal but decreased cardiac mRNAs. Extracts of the EBs in (A) were analyzed by reverse transcriptase–polymerase chain reaction (RT-PCR) to determine mRNA levels of the neuron-specific microtubule-associated protein 2 (*map2*) and cardiac-specific α-cardiac myosin heavy chain (*mhc*) genes. Glyceraldehyde-3-phosphate dehydrogenase (gapdh) was used as the loading control.

6 EBs that had been allowed to spontaneously differentiate. The region of the mouse *bmp-2* promoter encompassing the −656/−635 bp MEF2-binding site was successfully immunoprecipitated using anti-MEF2C antibody, indicating that MEF2C can indeed bind to the endogenous *bmp-2* promoter (Fig. 7C, top left panel). MEF2C did not bind to the promoter region of the control *bahd1* gene present on the same chromosome (Fig. 7C, top right). Further, SB203580 treatment inhibited the binding of MEF2C to the MEF2-binding site (Fig. 7C, bottom left). As a positive control, we examined the binding of MEF2C to the promoter of the mouse *mef2c* gene, which itself is a target of MEF2 transactivation. The resulting ChIP pattern was similar to that derived for *bmp-2* (Fig. 7C, middle). Collectively, these data indicate that BMP-2 is a direct transcriptional target of MEF2C.

Discussion

In this study, we analyzed the influence of the 3 major MAP kinases, ERK, JNK, and p38, on ES cell lineage commitment. Our results show that ERK and p38 MAPK play an essential role in the cardiomyogenesis of mES cells. An interesting cellular response of our work is that, at the same time as it promotes the induction of cardiomyocyte differentiation, p38 MAPK activity specifically inhibits neuronal differentiation. We demonstrate that p38 MAPK achieves these effects by activating the transcription factor MEF2C, which in turn directly regulates BMP-2 expression. Several previous studies also reported that p38 MAPK regulates both murine and human ES cell survival and lineage commitment, including cardiomyocyte differentiation [29–32]. Our work revealed the molecular mechanism of a switch between cardiomyocyte and neuronal commitment of mES cells.

The pyridinylimidazole compound SB203580 inhibits the catalytic activity of p38α and p38β MAPKs via competition for ATP, but SB203580 does not inhibit the closely related ERK or JNK enzymes or any other serine–threonine protein kinases [33]. Graichen *et al.* reported that SB203580 at concentrations lower than 10 μM induced cardiomyogenesis of human ES cells, whereas at concentrations more than 15 μM, it strongly inhibited cardiomyogenesis [30]. These results indicate the dose-dependent differences in lineage determination in human ES cells. However, we could not observe the phenomena using mES cells in the presence of SB203580 at concentrations of 5–20 μM (Fig. 3C). In our mES cell differentiation system, more than 90% EBs differentiated into cardiomyocytes in the absence of SB203580, and so it may be difficult to evaluate the enhanced induction of cardiomyogenesis by low concentrations of SB203580.

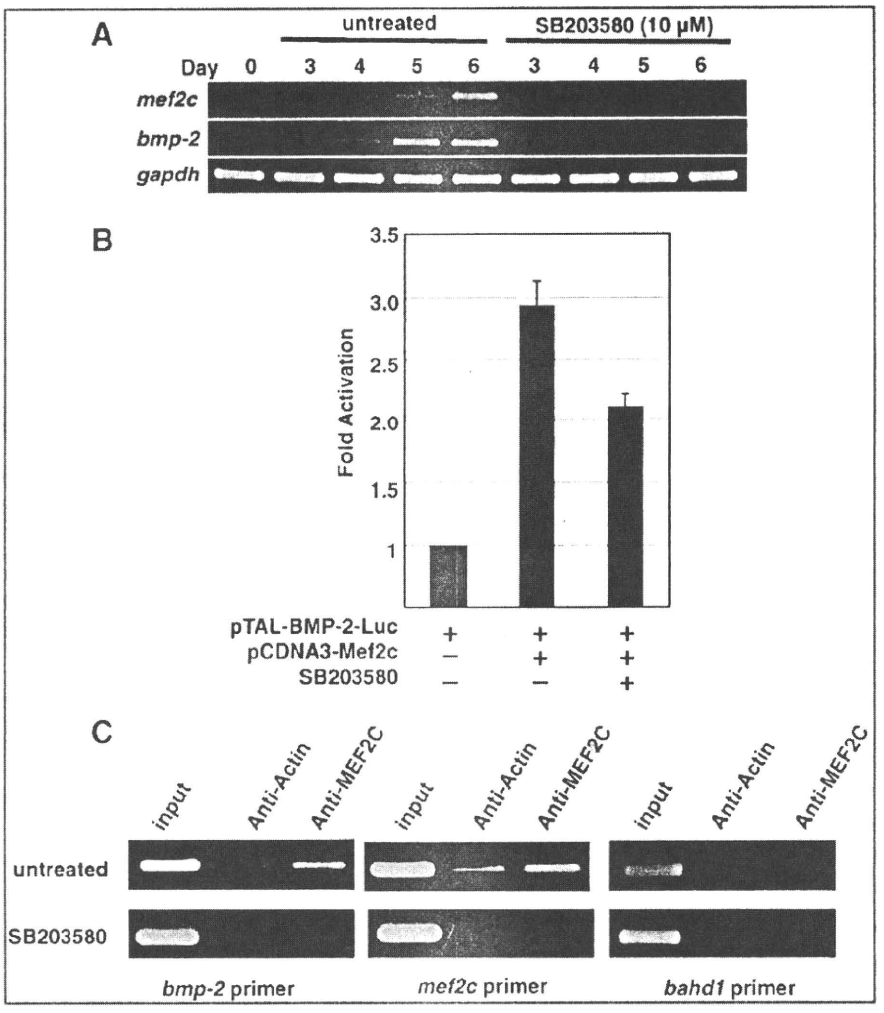

FIG. 7. Bone morphogenetic protein 2 (BMP-2) is a direct transcriptional target of myocyte enhancer factor 2C (MEF2C). **(A)** Similar patterns of *mef2c* and *bmp-2* expression. Embryoid bodies (EBs) were left untreated or treated with 10 μM SB203580 on days 3–6, and mRNA expression of *bmp-2* and *mef2c* was analyzed by reverse transcriptase–polymerase chain reaction (RT–PCR). Glyceraldehyde-3-phosphate dehydrogenase (gapdh) was used as the loading control. **(B)** MEF2C regulates *bmp-2* promoter activity. A proximal region (−1703/−1) of the mouse *bmp-2* promoter (containing the MEF2-binding site) was cloned into the pTAL-Luc reporter vector to yield pTAL-BMP-2-Luc, which was transfected into HeLa cells. HeLa cells were co-transfected with pcDNA3-Mef2c plasmid expressing MEF2C. Half of these co-transfected cells were treated with 10 μM SB203580. Luciferase activity was determined in cell lysates at 24 h after transfection. Results are expressed as the mean fold luciferase activation ± SD compared with pTAL-BMP-2-Luc-transfected HeLa cells. **(C)** MEF2C binds to the *bmp-2* promoter. EBs were left untreated or treated with 10 μM SB203580 on days 3–6. ChIP analyses of extracts were carried out on day 6 using anti-MEF2C antibody or control anti-actin IgG to immunoprecipitate chromatin. Precipitated DNAs were analyzed by PCR using primer pairs for the promoter regions of the *bmp-2*, *mef2c* (positive control), or bromo adjacent homology domain containing 1 (*bahd1*) (negative control) genes.

Consistent with our findings, Aouadi *et al.* have reported that loss of p38 MAPK activity due either to treatment with the chemical inhibitor PD169316 or to genetic p38α deficiency is sufficient to block cardiomyogenesis and induce a high level of neurogenesis [34]. These results clearly show that it is p38α that is mainly responsible for p38 MAPK functions during ES cell lineage commitment: the control of p38α activity constitutes an early switch, committing ES cells into either cardiomyogensesis (p38 on) or neurogenesis (p38 off). However, the molecular mechanism of p38 off-dependent neurogenesis was unclear.

P38 MAPK induces cell cycle exit and differentiation in many cell types, and activated p38 has been shown to phosphorylate several downstream signaling molecules important for cardiomyocyte differentiation and hypertrophy in murine P19 cells and mice [35–37]. In our study, we found that p38 MAPK is spontaneously activated between days 2 and 6 after the formation of EBs. Further, our data indicate that this spontaneous p38 MAPK activity is critical between days 3 and 4 for the cardiac commitment of ES cells. Inhibition of p38 MAPK activity at this early juncture drives ES cells toward the neuronal lineage. These findings stand in sharp contrast to those of other groups investigating the role of p38 MAPK in later stages of neuronal differentiation [38]. P38 MAPK activation is required for neurite formation and neuron survival in PC12 and P19 cells during the late stages of differentiation. Okamoto *et al.* reported that the p38α/MEF2 pathway prevents cell death during neuronal differentiation in P19 cells [39]. Thus, the role of p38 MAPK during the complex process of neuronal differentiation appears to be stage dependent.

BMPs are part of the larger superfamily of TGF-β ligands, which signal through a well-defined molecular pathway [21]. BMPs were found to be required for maintaining cultured mES cells in an undifferentiated state [40]. In our study, we demonstrate both that p38 MAPK regulates the expression of

BMP-2, and thereby controls mES cell lineage commitment, and that BMP-2 treatment inhibits SB203580-induced neuronal differentiation. Further, like SB203580, the exogenous BMP antagonist Noggin prevents the spontaneous differentiation of mES cells into cardiomyocytes and promotes neuronal differentiation. These data suggest a dynamic role for BMP in specifying cell fate and emphasize that defining the molecular context of BMP signaling is critical for understanding how ES cells are regulated at a physiological level.

MEF2C is an important transcription factor that transactivates many genes encoding cardiac structural proteins, and p38 MAPK is a well-known regulator of MEF2C [14,41–43]. Gene-targeted mouse embryos lacking MEF2C have cardiogenic defects [17]. BMP-2 is also required for cardiogenesis, and BMP2-deficient embryos exhibit an early defect in cardiac development [44]. In our study, we found that BMP-2 is a direct transcriptional target of MEF2C, and that p38 MAPK may regulate BMP-2 by controlling MEF2C activation. However, we found that simple stimulation of ES cells with BMP-2 did not augment cardiomyocyte generation (data not shown), suggesting that BMP-2 is essential but not sufficient for cardiac induction. It is likely that other MEF2C-dependent genes encoding cardiac structural proteins are also required for normal cardiac development. It will be interesting to investigate whether MEF2C$^{-/-}$ ES cells can differentiate spontaneously into neurons. Additionally, unknown factors in FBS contribute to the frequency of beating EBs and play important roles in cell lineage commitment.

In conclusion, our study has revealed an intriguing role for p38 MAPK as a cell fate switch during ES cell differentiation. The choice between cardiac and neuronal cell development depends on the early stage function of BMP-2, whose expression in turn depends on transactivation by the p38 MAPK target MEF2C.

Acknowledgments

This work was supported by research grants from the Ministry of Education, Culture, Sports, Science, and Technology of Japan and the Japanese Society for the Promotion of Science. The authors are grateful to numerous members of the Nishina and Katada Laboratories for critical reading of this manuscript and helpful discussions.

Author Disclosure Statement

No competing financial interests exist.

References

1. Evans MJ and M Kaufman. (1981). Establishment in culture of pluripotential cells from mouse embryos. Nature 292:154–156.
2. Martin GR. (1981). Isolation of a pluripotent cell line from early mouse embryos cultured in medium conditioned by teratocarcinoma stem cells. Proc Natl Acad Sci USA 78:7634–7638.
3. Smith AG, JK Heath, DD Donaldson, GG Wong, J Moreau, M Stahl and D Rogers. (1988). Inhibition of pluripotential embryonic stem cell differentiation by purified polypeptides. Nature 336:688–690.
4. Williams RL, DJ Hilton, S Pease, TA Willson, CL Stewart, DP Gearing, EF Wagner, D Metcalf, NA Nicola and NM Gough. (1988). Myeloid leukaemia inhibitory factor maintains the developmental potential of embryonic stem cells. Nature 336:684–687.
5. Smith AG. (2001). Embryo-derived stem cells: of mice and men. Annu Rev Cell Dev Biol 17:435–462.
6. Davis RJ. (2000). Signal transduction by the JNK group of MAP kinases. Cell 103:239–252.
7. Chang L and M Karin. (2001). Mammalian MAP kinase signalling cascades. Nature 410:37–40.
8. Han J, JD Lee, L Bibbs and RJ Ulevitch. (1994). A MAP kinase targeted by endotoxin and hyperosmolarity in mammalian cells. Science 265:156–160.
9. Lee JC, JT Laydon, PC McDonnell, TF Gallagher, S Kumar, D Green, D McNulty, MJ Blumenthal, JR Keys, SW Landvatter, JE Strickler, MM Mclaughlin, IR Siemens, SM Fisher, GP Livi, JR White, JL Adama and PR Young. (1994). A protein kinase involved in the regulation of inflammatory cytokine biosynthesis. Nature 372:739–746.
10. Wang XS, K Diener, CL Manthey, S Wang, B Rosenzweig, J Bray, J Delaney, CN Cole, PY Chan-Hui, N Mantlo, HS Lichenstein, M Zukowski and Z Yao. (1997). Molecular cloning and characterization of a novel p38 mitogen-activated protein kinase. J Biol Chem 272:23668–23674.
11. Tamura K, T Sudo, U Senftleben, AM Dadak, R Johnson and M Karin. (2000). Requirement for p38alpha in erythropoietin expression: a role for stress kinases in erythropoiesis. Cell 102:221–231.
12. Mudgett JS, J Ding, L Guh-Siesel, NA Chartrain, L Yang, S Gopal and MM Shen. (2000). Essential role for p38alpha mitogen-activated protein kinase in placental angiogenesis. Proc Natl Acad Sci USA 97:10454–10459.
13. Beardmore VA, HJ Hinton, C Eftychi, M Apostolaki, M Armaka, J Darragh, McIlrath J, JM Carr, LJ Armit, C Clacher, L Malone, G Kollias and JS Arthur. (2005). Generation and characterization of p38beta (MAPK11) gene-targeted mice. Mol Cell Biol 23:10454–10464.
14. Han J, Y Jiang, Z Li, VV Kravchenko and RJ Ulevitch. (1997). Activation of the transcription factor MEF2C by the MAP kinase p38 in inflammation. Nature 386:296–299.
15. Martin JF, JM Miano, CM Hustad, NG Copeland, NA Jenkins and EN Olson. (1994). A Mef2 gene that generates a muscle-specific isoform via alternative mRNA splicing. Mol Cell Biol 14:1647–1656.
16. Black BL and EN Olson. (1998). Transcriptional control of muscle development by myocyte enhancer factor-2 (MEF2) proteins. Annu Rev Cell Dev Biol 14:167–196.
17. Lin Q, J Schwarz, C Bucana and EN Olson. (1997). Control of mouse cardiac morphogenesis and myogenesis by transcription factor MEF2C. Science 276:1404–1407.
18. Bi W, CJ Drake and JJ Schwarz. (1999). The transcription factor MEF2C-null mouse exhibits complex vascular malformations and reduced cardiac expression of angiopoietin 1 and VEGF. Dev Biol 211:255–267.
19. Czyz J and A Wobus. (2001). Embryonic stem cell differentiation: the role of extracellular factors. Differentiation 68:167–174.
20. Tiedemann H, M Asashima, H Grunz and W Knöchel. (2001). Pluripotent cells (stem cells) and their determination and differentiation in early vertebrate embryogenesis. Dev Growth Differ 43:469–502.
21. Wozney JM, V Rosen, AJ Celeste, LM Mitsock, MJ Whitters, RW Kriz, RM Hewick and EA Wang. (1988). Novel regulators of bone formation: molecular clones and activities. Science 242:1528–1534.

22. Attisano L and JL Wrana. (2002). Signal transduction by the TGF-beta superfamily. Science 296:1646–1647.
23. Shah NM, AK Groves and DJ Anderson. (1996). Alternative neural crest cell fates are instructively promoted by TGFbeta superfamily members. Cell 85:331–343.
24. Nishina H, KD Fischer, L Radvanyi, A Shahinian, R Hakem, EA Rubie, A Bernstein, TW Mak, JR Woodgett and JM Penninger. (1997). Stress-signaling kinase Sek1 protects thymocytes from apoptosis mediated by CD95 and CD3. Nature 385:350–353.
25. Takayanagi H, S Kim, T Koga, H Nishina, M Isshiki, H Yoshida, A Saiura, M Isobe, T Yokochi, J Inoue, EF Wagner, TW Mak, T Kodama and T Taniguchi. (2002). Induction and Activation of the Transcription Factor NFATc1 (NFAT2) Integrate RANKL Signaling. Dev Cell 3:889–901.
26. Shimizu N, H Watanabe, J Kubota, J Wu, R Saito, T Yokoi, T Era, T Iwatsubo, T Watanabe, S Nishina, N Azuma, T Katada and H Nishina. (2009). Pax6-5a promotes neuronal differentiation of murine embryonic stem cells. Biol Pharm Bull 32:999–1003.
27. Saito R, T Yamasaki, Y Nagai, J Wu, H Kajiho, T Yokoi, E Noda, S Nishina, H Niwa, N Azuma, T Katada and H Nishina. (2009). CrxOS maintains self-renewal capacity of murine embryonic stem cells. Biochem Biophys Res Commun 390:1129–1135.
28. Ura S, H Nishina, Y Gotoh and Katada T. (2007). Activation of the JNK patyway by MST1 is essential and sufficient for the induction of chromatin condensation during apoptosis. Mol Cell Biol 27:5514–5522.
29. Androutsellis-Theotokis A, RR Leker, F Soldner, DJ Hoeppner, R Ravin, SW Poser, MA Rueger, SK Bae, R Kittappa and RD McKay. (2006). Notch signalling regulates stem cell numbers *in vitro* and *in vivo*. Nature 442:823–826.
30. Graichen R, X Xu, SR Braam, T Balakrishnan, S Norfiza, S Sieh, SY Soo, SC Tham, C Mummery, A Colman, R Zweigerdt and BP Davidson. (2008). Enhanced cardiomyogenesis of human embryonic stem cells by a small molecular inhibitor of p38 MAPK. Differentiation 76:357–370.
31. Binétruy B, L Heasley, F Bost, L Caron and M Aouadi. (2007). Concise review: regulation of embryonic stem cell lineage commitment by mitogen-activated protein kinases. Stem Cells 25:1090–1095.
32. Ding L, XG Liang, Y Hu, DY Zhu and YJ Lou. (2008). Involvement of p38MAPK and reactive oxygen species in icariin-induced cardiomyocyte differentiation of murine embryonic stem cells *in vitro*. Stem Cells Dev 17:751–760.
33. Cuenda A, J Rouse, YN Doza, R Meier, P Cohen, TF Gallagher, PR Young and JC Lee. (1995). SB 203580 is a specific inhibitor of a MAP kinase homologue which is stimulated by cellular stresses and interleukin-1. FEBS Lett 364:229–233.
34. Aouadi M, F Bost, L Caron, K Laurent, Y Le Marchand Brustel and B Binétruy. (2006). p38 mitogen-activated protein kinase activity commits embryonic stem cells to either neurogenesis or cardiomyogenesis. Stem Cells 24:1399–1406.
35. Davidson SM and M Morange. (2000). Hsp25 and the p38 MAPK pathway are involved in differentiation of cardiomyocytes. Dev Biol 218:146–160.
36. Zetser A, E Gredinger and E Bengal. (1999). p38 mitogen-activated protein kinase pathway promotes skeletal muscle differentiation. Participation of the Mef2c transcription factor. J Biol Chem 274:5193–5200.
37. Liang Q and JD Molkentin. (2003). Redefining the roles of p38 and JNK signaling in cardiac hypertrophy: dichotomy between cultured myocytes and animal models. J Mol Cell Cardiol 35:1385–1394.
38. Takeda K and H Ichijo. (2002). Neuronal p38 MAPK signalling: an emerging regulator of cell fate and function in the nervous system. Genes Cells 7:1099–1111.
39. Okamoto S, D Krainc, K Sherman and SA Lipton. (2000). Antiapoptotic role of the p38 mitogen-activated protein kinase-myocyte enhancer factor 2 transcription factor pathway during neuronal differentiation. Proc Natl Acad Sci USA 97:7561–7566.
40. Ying QL, J Nichols, I Chambers and A Smith. (2003). BMP induction of Id proteins suppresses differentiation and sustains embryonic stem cell self-renewal in collaboration with STAT3. Cell 115:281–292.
41. Zhao M, L New, VV Kravchenko, Y Kato, H Gram, F di Padova, EN Olson, RJ Ulevitch and J Han. (1999). Regulation of the MEF2 family of transcription factors by p38. Mol Cell Biol 19:21–30.
42. Yang SH, A Galanis and AD Sharrocks. (1999). Targeting of p38 mitogen-activated protein kinases to MEF2 transcription factors. Mol Cell Biol 19:4028–4038.
43. Wu Z, PJ Woodring, KS Bhakta, K Tamura, F Wen, JR Feramisco, M Karin, JY Wang and PL Puri. (2000). p38 and extracellular signal-regulated kinases regulate the myogenic program at multiple steps. Mol Cell Biol 20:3951–3964.
44. Zhang H and A Bradley. (1996). Mice deficient for BMP2 are nonviable and have defects in amnion/chorion and cardiac development. Development 122:2977–2986.

Address correspondence to:
Prof. Hiroshi Nishina
Department of Developmental and Regenerative Biology
Medical Research Institute
Tokyo Medical and Dental University
1-5-45 Yushima, Bunkyo-ku
Tokyo 113-8510
Japan

E-mail: nishina.dbio@mri.tmd.ac.jp

Received for publication February 6, 2010
Accepted after revision April 22, 2010
Prepublished on Liebert Instant Online April 22, 2010

Cell

A Global In Vivo *Drosophila* RNAi Screen Identifies *NOT3* as a Conserved Regulator of Heart Function

G. Gregory Neely,[1,16] Keiji Kuba,[2,16,*] Anthony Cammarato,[3,16] Kazuya Isobe,[2,4] Sabine Amann,[1] Liyong Zhang,[7] Mitsushige Murata,[8] Lisa Elmén,[3] Vaijayanti Gupta,[9] Suchir Arora,[9] Rinku Sarangi,[9] Debasis Dan,[9] Susumu Fujisawa,[2] Takako Usami,[5] Cui-ping Xia,[1] Alex C. Keene,[10] Nakissa N. Alayari,[3] Hiroyuki Yamakawa,[8] Ulrich Elling,[1] Christian Berger,[1] Maria Novatchkova,[1] Rubina Koglgruber,[1] Keiichi Fukuda,[8] Hiroshi Nishina,[6] Mitsuaki Isobe,[4] J. Andrew Pospisilik,[1] Yumiko Imai,[2] Arne Pfeufer,[11,12] Andrew A. Hicks,[13] Peter P. Pramstaller,[13,14,15] Sai Subramaniam,[9] Akinori Kimura,[5] Karen Ocorr,[3] Rolf Bodmer,[3,*] and Josef M. Penninger[1,*]

[1]Institute of Molecular Biotechnology (IMBA) of the Austrian Academy of Sciences, Dr. Bohr Gasse 3-5, A-1030 Vienna, Austria
[2]Department of Biological Informatics and Experimental Therapeutics, Akita University Graduate School of Medicine, 1-1-1 Hondo, Akita 010-8543, Japan
[3]Development and Aging Program, Del E. Webb Neuroscience, Aging, and Stem Cell Research Center, Sanford-Burnham Medical Research Institute, La Jolla, CA 92037, USA
[4]Department of Cardiology
[5]Department of Molecular Pathogenesis, Medical Research Institute
[6]Department of Developmental and Regenerative Biology, Medical Research Institute
Tokyo Medical and Dental University, Bunkyo-ku, Tokyo 113-8510, Japan
[7]Division of Cardiology, Toronto General Hospital, University Health Network, University of Toronto, Canada
[8]Department of Regenerative Medicine and Advanced Cardiac Therapeutics, Keio University School of Medicine, 160-8582 Tokyo, Japan
[9]Strand Life Sciences, 237 C V Raman Avenue, Rajmahal Vilas, 560024 Bangalore, India
[10]Biology Department, New York University, 100 Washington Square East, New York, NY 10003, USA
[11]Institute of Human Genetics, Technische Universität München, D-81675 Munich, Germany
[12]Institute of Human Genetics, Helmholtz Center München, D-85764 Neuherberg, Germany
[13]Institute of Genetic Medicine, European Academy Bozen/Bolzano, 39100 Bolzano, Italy
[14]Department of Neurology, General Central Hospital, 39100 Bolzano, Italy
[15]Department of Neurology, University of Lübeck, 23538 Lübeck, Germany
[16]These authors contributed equally to this work
*Correspondence: kuba@med.akita-u.ac.jp (K.K.), rolf@burnham.org (R.B.), josef.penninger@imba.oeaw.ac.at (J.M.P.)
DOI 10.1016/j.cell.2010.02.023

SUMMARY

Heart diseases are the most common causes of morbidity and death in humans. Using cardiac-specific RNAi-silencing in *Drosophila*, we knocked down 7061 evolutionarily conserved genes under conditions of stress. We present a first global roadmap of pathways potentially playing conserved roles in the cardiovascular system. One critical pathway identified was the CCR4-Not complex implicated in transcriptional and posttranscriptional regulatory mechanisms. Silencing of CCR4-Not components in adult *Drosophila* resulted in myofibrillar disarray and dilated cardiomyopathy. Heterozygous *not3* knockout mice showed spontaneous impairment of cardiac contractility and increased susceptibility to heart failure. These heart defects were reversed via inhibition of HDACs, suggesting a mechanistic link to epigenetic chromatin remodeling. In humans, we show that a common *NOT3* SNP correlates with altered cardiac QT intervals, a known cause of potentially lethal ventricular tachyarrhythmias. Thus, our functional genome-wide screen in *Drosophila* can identify candidates that directly translate into conserved mammalian genes involved in heart function.

INTRODUCTION

Cardiovascular diseases are the most common cause of death in North America and Europe (Yusuf et al., 2001) killing more than 860,000 people annually in the United States (A.H.A., 2005; Lloyd-Jones et al., 2009). Moreover, 80 million people in the United States are estimated to suffer from cardiovascular diseases (A.H.A., 2005; Lloyd-Jones et al., 2009). Known or associated causes of cardiovascular disease include diabetes mellitus, inflammation, high cholesterol, hypertension, overweight and obesity, physical inactivity, or smoking (A.H.A., 2005; Lloyd-Jones et al., 2009). Although there have been great advances in the understanding of heart failure in recent decades (Mudd and Kass, 2008), there is still a gap in understanding the genetic causes and an unmet need for better therapies. In particular, the complex interplay of lifestyle, genetic susceptibilities,

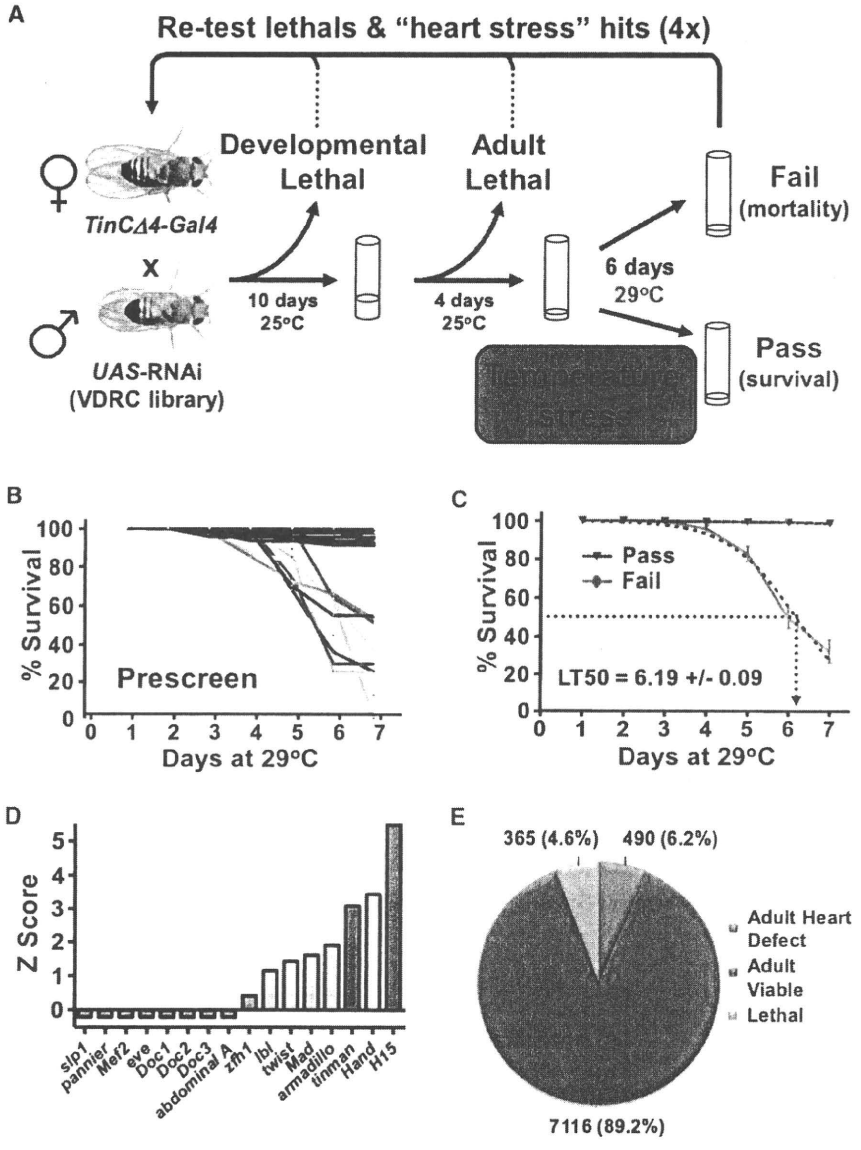

Figure 1. Genome-wide Screen for Conserved Heart Genes

(A) Schematic for screen setup. *TinΔ4-Gal4*, a cardiac tissue specific driver, was used to drive conserved *UAS*-RNAi hairpins in the developing heart. Developmental lethality and baseline adult viability was scored. Viable adult flies were then given a heart stress (continued exposure to 29°C) and survival was scored on day 6. Fly lines showing a potential developmental or heart function phenotype were then retested to confirm the candidate gene.

(B) Eighty randomly selected *UAS*-RNAi lines were crossed to *TinCΔ4-Gal4* and evaluated for adult lethality after an increase in ambient temperature as a cardiac stressor. Lines were either viable (black) or died starting around day 3. Data from individual lines are shown as percent survival on the indicated days.

(C) Mean responses from viable and failing (death after exposure to 29°C) flies revealed an average lethal time at which 50% of failing flies died (LT50) of 6.19 days.

(D) Efficacy of *TinCΔ4-Gal4* x *UAS*-RNAi lines to knock down transcription factors known to play a role in heart formation.

(E) With this system, a genome-wide screen was performed to search for conserved candidate genes for adult heart function under conditions of cardiac stress; 4.6% *TinCΔ4-Gal4* x *UAS*-RNAi lines were developmental lethal. Among the 7971 viable lines, 490 transformant lines exhibited significantly increased death (Z score >3, determined on day 6 after shifting the ambient temperature to 29°C).

See also Figure S1 and Tables S1 and S2.

diseases, and aging have made it difficult to understand the underlying pathogenic principles (Yusuf et al., 2001). In addition to large-scale genetic mapping and phenotyping in humans (Gordon et al., 1977; Morita et al., 2005; Nabel, 2003), a genetic dissection of the cardiovascular system in less complex model organisms would greatly facilitate the understanding of basic controls of cardiac physiology and mechanisms of disease.

Multiple proteins that control contraction in cardiomyocytes are highly conserved between species. For instance, the fly heart is capable of spontaneous rhythmic activity required for the circulation of hemolymph, and the same genes control heart rhythm in humans and flies (Ocorr et al., 2007a). In aging flies, the heartbeat becomes irregular with increased episodes of arrhythmias (Ocorr et al., 2007b), reminiscent of increased atrial fibrillation and heart failure in older humans (Lakatta and Levy, 2003). Moreover, genes involved in specification and differentiation of the heart are also conserved between *Drosophila* and mammals (reviewed in Bodmer, 1995; Cripps and Olson, 2002; Ocorr et al., 2007a). Mutations in subunits of repolarizing voltage gated potassium channels I_{Kr} (*eag, KCNH2*) and I_{Ks} (*kvLQT1, KCNQ1*) perturb heart function in *Drosophila* and in vertebrates can cause long QT syndrome (Ocorr et al., 2007b; Sanguinetti and Tristani-Firouzi, 2006). Moreover, the sarco-endoplasmic reticulum Ca^{2+}-ATPase (*serca2a*, *ATP2A2*) and the Ca^{2+}-channel *Cacophony* control heart function also in *Drosophila* (Ray and Dowse, 2005; Sanyal et al., 2006). Thus, *Drosophila* has become a powerful genetic model system to identify conserved genes involved in heart function.

RESULTS

A *Drosophila* High-Throughput Assay to Identify Candidate Heart Genes

To identify candidate genes for heart development and heart function (Figure 1A), we used cardiac tissue-specific RNA interference (RNAi) silencing of all genes that we identified as showing possible conservation between mammalian species and *Drosophila melanogaster* (Table S1, part A, available online).

TinCΔ4-Gal4 specifically drives expression in cardioblasts (Lo and Frasch, 2001) and has been previously used to study genes involved in heart function of the adult fly (Qian et al., 2008). Because RNAi-mediated downregulation of gene expression in many cases permits the circumvention of lethality commonly associated with classical mutations (Dietzl et al., 2007), cardiac tissue-specific *TinCΔ4-Gal4* RNAi-mediated gene silencing therefore allowed us to assay the functional roles of the respective target genes in adult flies. Since elevated ambient temperature results in an increase in *Drosophila* heart rate (Paternostro et al., 2001; Ray and Dowse, 2005), we combined cardiac tissue-specific RNAi knockdown with an increased ambient temperature to reveal cardiac phenotypes under conditions of stress. Elevated temperature also enhances the activity of the UAS/GAL4 system, without affecting survival within the timeframe of the experiment (Figure S1A).

To evaluate the efficacy of this experimental setup (Figure 1A), we performed a prescreen with 80 randomly selected genes that were targeted by *TinCΔ4-Gal4* RNAi (Table S1, part B). Whereas ~10% of these *TinCΔ4-Gal4* RNAi lines started to die at the increased ambient temperature, the vast majority survived for more than 7 days (Figure 1B). From these pilot experiments, we calculated an average time of 6.19 days at which 50% of flies among the susceptible lines had died (lethal time 50 [LT50]) (Figure 1C). Thus, our large-scale genome-wide screen was carried out at 29°C and lethality was recorded for each line at day 6. As a control, *TinCΔ4-Gal4* RNAi knockdown of known cardiogenic transcription factors resulted in viable lines at 25°C (data not shown), but a shift to 29°C resulted in increased death of nearly half of the transcription factor RNAi lines tested, including *Tinman*, *Hand*, and *H15* (*neuromancer-1/Tbx20*) (Figure 1D). Cardiac knockdown of *pannier/Gata4* and the *Doc* genes (*Tbx5/6*) did not cause premature lethality at 29°C, even though they are known to contribute to adult heart function (Qian and Bodmer, 2009; Qian et al., 2008). As negative controls, we used RNAi lines targeting *eve* and *zfh-1*, which are not expressed in the myocardium targeted by *TinCΔ4-Gal4* (Figure 1D). Thus, we have set up a model system that allows for efficient high-throughput screening and has the capacity to pick up known heart genes.

A Genome-wide In Vivo Fly RNAi Screen for Conserved Genes

In total we screened 8417 transgenic RNAi lines corresponding to 7061 conserved genes for potential developmental and adult heart functional defects (Table S1, part C). We only included 7971 lines representing 6751 genes that fit the previously defined criteria of specificity (Dietzl et al., 2007) for further analyses, i.e., only lines with an S19 score ≥ 0.8 and having six or fewer CAN repeats were considered specific (Table S1, part D). Progeny of each RNAi line crossed to *TinCΔ4-Gal4* were first monitored for viability (reared at 25°C). Among these 7971 RNAi lines, 365 lines resulted in lethality (Figure 1E and Table S1, part E), indicating that many of these genes function in heart development. Developmental lethality was further staged as lethal (embryonic lethal or we never observed any offspring), larval lethal, pupal lethal, or early adult (within 4 days after eclosion) lethal (Table S1, part F).

To identify candidate genes for adult heart function, we assayed 7804 adult *TinCΔ4-Gal4* RNAi progeny (Dietzl et al., 2007) for survival after shifting the flies to 29°C (Figures S1B–S1D). To categorize our hits from the screen, we used the Z score, which is a measure of the distance in standard deviations of a sample from the mean. All RNAi lines with a Z score of 2 in the primary screen were tested on average 4.18 independent times (an average of 90 flies per genotype) using in some cases second RNAi transformants to control for transgenic insertion effects and second independent RNAi hairpins to target a different region of the gene (Table S2). After repeated screening, we identified 498 genes that passed the more stringent Z score of 3 (Figure 1E and Table S2), indicating that these hits exhibit a death score of three standard deviations from the mean. Using gene ontology (GO) annotations, our candidate hits were classified according to their predicted biological processes (BP), molecular functions (MF), and cellular components (CC). Of the classified genes, those involved in signaling, ion transporter activity, metabolism and mitochondrial structure, development and morphogenesis, transcriptional regulation, or nucleic acid binding were highly represented among the entire data set (Figure S2 and Table S4, part A). To remove any artificial bias in the gene list created by the ad hoc Z score cutoff >3, we performed a gene set analysis (GSA) to confirm enrichment of selected GO terms (Table S4, part B). In addition, 121 candidate heart genes had no annotated function by GO. With panther (http://www.pantherdb.org/), we were able to functionally annotate 116 of these genes (Table S4, part C).

Given that the RNAi library screened is known to generate a level of false negative phenotypes because of inefficient targeting of genes to levels required to reveal phenotypes (Dietzl et al., 2007), and based on the assumption that our candidate heart hits perform some of their functions in protein complexes, we next identified first-degree binding partners (Table S4, part D). Using this list of primary heart hits and their binding partners, we performed fly KEGG pathway analyses. Moreover, we included developmental lethal hits to generate a global interaction network. KEGG analyses showed enrichment of multiple pathways, such as mTOR signaling and PI3K/AKT, amino acid metabolism, JAK-STAT signaling, ErbB signaling, the Wnt, Notch, hedgehog, or TGFβ pathways, protein degradation, VEGF signaling, DNA repair, and calcium homeostasis (Table S3 and Table S4, part E). Besides the identification of multiple known genes, our screen has also revealed hundreds of candidate genes and pathways that have not been previously associated with heart function.

A Global View of Heart Function

To extend our *Drosophila* results to mammalian systems, we used the power of data mining and bioinformatics at a global systems level. Potential mouse and human orthologs of our candidate heart screen hits were evaluated for GO enrichment. The GO analyses of the human and mouse orthologs showed marked enrichment of genes involved in PIP3 and calcium signaling, ion transporter activity, metabolism, development, fatty acid metabolism, and muscle contraction (Table S4, part F). We next performed KEGG pathway as well as Broad Institute C2 gene set analysis on the mouse and human orthologs and

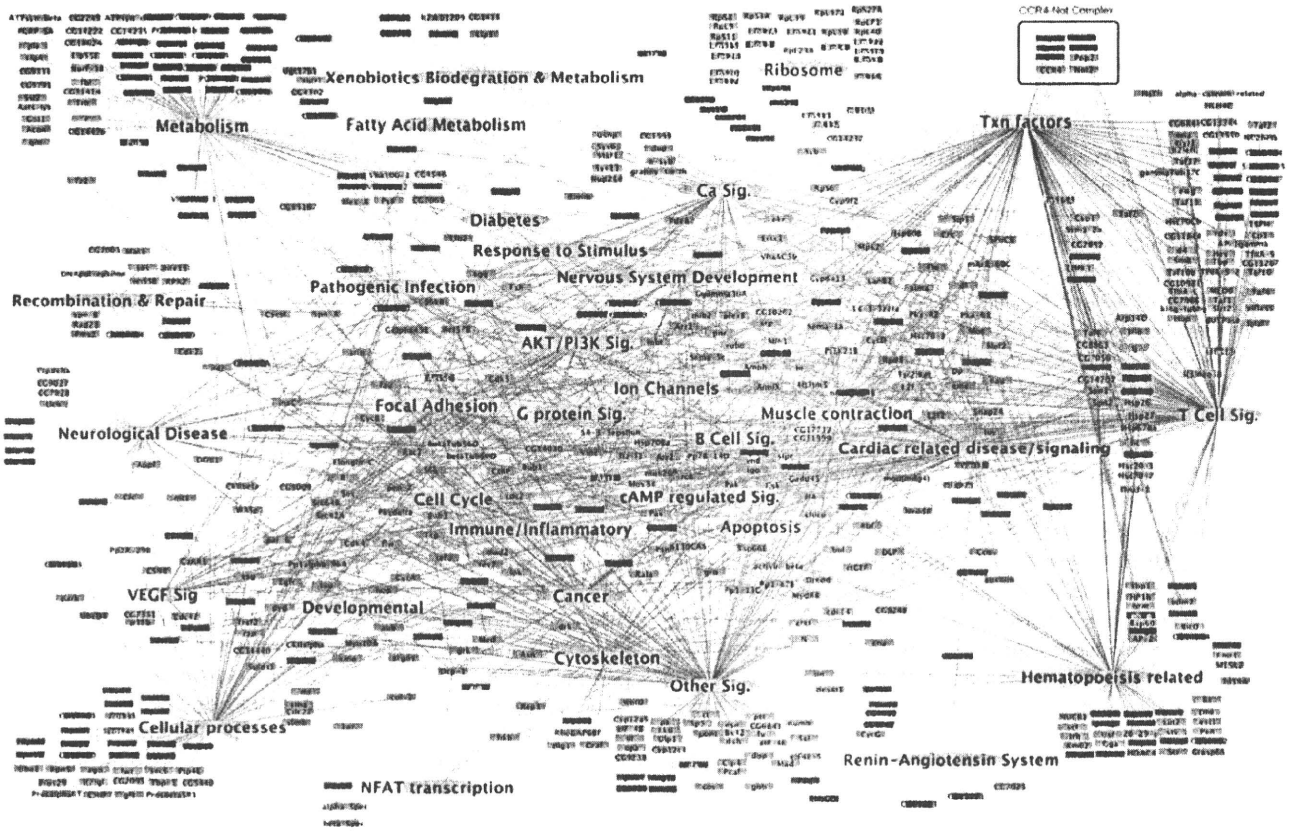

Figure 2. A Global Network of Heart Function

The systems network includes data from the significantly enriched *Drosophila* KEGG and mouse and human KEGG and C2 data sets. Pathways and gene sets from the same biological processes were grouped into common functional categories. Orange nodes represent statistically enriched functional categories of pathways, red nodes represent direct primary fly RNAi hits, green nodes represent their first degree binding partners, and blue nodes indicate genes that were scored as developmentally lethal in our *Drosophila* heart screen. Lines indicate associations of the genes to the appropriate functional category. All KEGG pathways and selected C2 gene sets have been represented in the systems map. See also Tables S3, S4, and S5.

their first-degree binding partners. Based on the mammalian KEGG (Table S4, part E) and C2 (Table S4, part G) analyses, we found significant enrichment for gene sets involved in signaling, metabolism, ion channels, inflammation, aging, and transcription.

To generate a network map that includes our functional data in *Drosophila*, their human and mouse orthologs, and first-degree binding partners, we combined KEGG pathways from *Drosophila*, mouse, and human with relevant gene sets from the Broad Institute C2 annotations (Table S4). A combined systems map and the interactions between the individual genes in the indicated nodes are shown in Figure 2 and Table S4, part H. A systems map using only direct screening hits was also generated, yielding a comparable network map (Table S3). Importantly, by using this network approach, we identified multiple pathways known to play key roles in heart function and cardiovascular disease. For instance, we found significant enrichment in NFAT transcription, AKT activation, and PI3K signaling, calcium signaling and muscle contraction, GPCR- and cAMP signaling, ion channels and proton-transporting ATPase complexes, and transcription. We also found associations with the renin-angiotensin system, a key pathway involved in cardiovascular function in humans (Figure 2 and Table S4, part H). In support of our network approach, advanced data mining revealed that 171 of our primary fly hits and their first-degree binding partners corresponded to mouse knockouts with known cardiovascular phenotypes (Table S5). Thus, our genome-wide screen for candidate heart genes and in silico analyses provides a first attempt at a global roadmap of essential molecular components and key pathways potentially involved in heart function and cardiac failure.

RNAi Silencing of *not3* and *UBC4* Results in Dilated Cardiomyopathy in *Drosophila*

One of the pathways we found in our global network analysis was the CCR4-Not complex (Figure 2 and Table S3). Intriguingly, among the eight members of this complex assayed, we hit the subunits *not1*, *not3* (*not3/5* in fly), *not4*, *UBC4*, and *Hsp83* (Figure 3A). In addition, the subunits *not2* and *CG8759* were "weak" hits (Figure 3A). The CCR4-Not complex was first identified in yeast (Denis, 1984) and is highly conserved in evolution (Albert et al., 2000). Components of the CCR4-Not complex

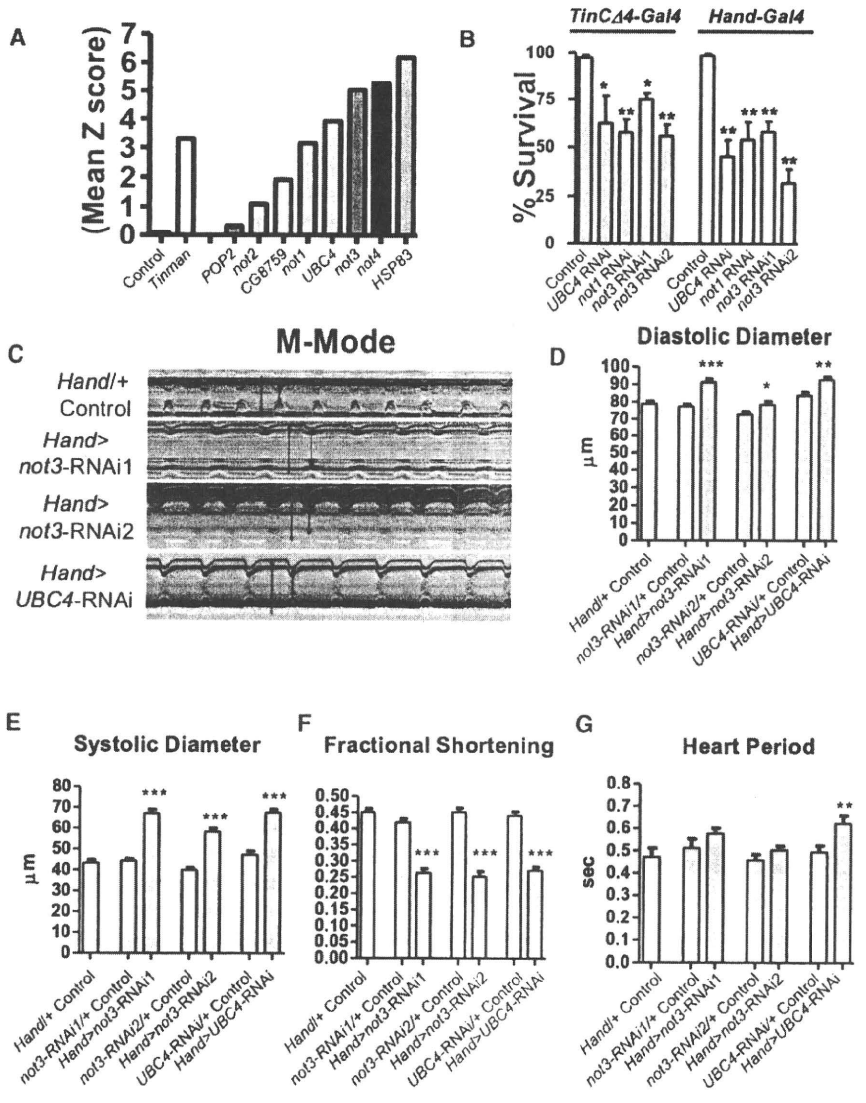

Figure 3. The CCR4-Not Complex Is a Central Regulator of Adult Heart Function, and Loss of not3 Results in Dilated Cardiomyopathy in *Drosophila*

(A) Mean Z scores for *TinCΔ4-Gal4* x *UAS*-RNAi lines targeting the indicated members of the fly CCR4-Not complex. A negative control (w^{1118} [isogenic to the RNAi library] X *TinΔ4-Gal4*) and the positive control *Tinman* RNAi line are shown.

(B) *not1*, *not3*, and *UBC4* are essential for proper adult heart function in both *Tinman*- and *Hand*-expressing cells. Data are shown as mean ± SEM for at least three replicates. RNAi1 and RNAi2 indicate different transgenic hairpins targeting *not3* . *p < 0.05, **p < 0.01 by ANOVA.

(C) One-week-old adult flies with *Hand-Gal4* driving *not3* or *UBC4* cardiac-specific knockdown exhibit impaired heart function. M modes provide traces of the heart contractions to document the movements in a 1 pixel wide region of the heart tube over time. *HandG4/+* control are the progeny of *Hand-Gal4* crossed to w^{1118}. *Hand>Not3* complex flies are the progeny of *Hand-Gal4* crossed to either *UAS-not3*-RNAi (−1 or −2) or to UAS-*UBC4*-RNAi lines. Fly heart analysis was performed with a MatLab-based image analysis program (Fink et al., 2009; Ocorr et al., 2007b). M modes of the RNAi knockdown hearts reveal dilated diastolic and systolic diameters (double-headed red arrows) and reduced shortening properties (difference between diameters) when compared to M modes of control hearts. Each trace represents a 5 s recording.

(D–G) *Not3* or *UBC4* heart-specific knockdown perturbs several indices of cardiac performance. Progeny of *Hand-Gal4* crossed to two different *UAS-not3*-RNAi lines or an *UAS-UBC4*-RNAi line (experimental) and w^{1118} crossed to *UAS*-RNAi or *Hand-Gal4* driver (controls) were used for these experiments as in (C). *not3* and *UBC4* knockdown led to significantly wider diastolic (D) and systolic (E) diameters, and as a result significantly depressed (F) fractional shortening in all experimental lines relative to controls. *not3* knockdown trended toward a slight lengthening in the heart period (time between consecutive diastolic intervals), while *UBC4* knockdown led to a significant increase in heart period (G). Mean values ± SEM are shown for each group (n = 29–40). Unpaired t tests were performed between each *Hand-Gal4>UAS*-RNAi and each corresponding *UAS*-RNAi/+ control (progeny of w^{1118} crossed to *UAS*-RNAi line). Additionally, one-way ANOVAs with Bonferroni multiple comparison tests revealed no significant differences between the *HandG4/+* control and all *UAS*-RNAi/+ control lines, for any cardiac parameter measured.

*p < 0.05, **p < 0.01, ***p < 0.001. See also Figure S3 and Movie S1.

have not yet been associated with cardiovascular function. We therefore retested components of this pathway using *TinCΔ4-Gal4*-driven knockdown in the heart, which confirmed the phenotype (Figure 3B). Moreover, use of a second heart driver, *Hand-Gal4*, which is expressed with high specificity in myocardial and pericardial cells throughout development and in the adult fly heart (Han and Olson, 2005), showed that silencing of *not1*, *not3*, and *UBC4* resulted in early death when adult flies were shifted to 29°C (Figure 3B).

Since *not3* RNAi gave a strong phenotype with two different *UAS*-RNAi lines (Figure 3B), we focused on the CCR4-Not component *not3*. Cardiac-specific knockdown of *not3* with two different RNAi lines (*Hand>not3*-RNAi: progeny from *Hand*-Gal4 crossed to *UAS-not3*-RNAi) significantly increased both diastolic and systolic diameters and resulted in reduced systolic fractional shortening relative to control flies (Figures 3C–3F and Movie S1). Hearts with cardiac *not3* knockdown also showed slight increases in heart periods (Figure 3G); however, this was not statistically significant. Fluorescent microscopy revealed that *not3* RNAi lines exhibit marked myofibrillar disarray, especially in the conical chamber (Figures 4A–4D). Heart-restricted *not3*-RNAi-mediated knockdown was confirmed by qRT-PCR (Figure S3). In addition, we observed transcriptional downregulation of the Sarcoplasmic/endoplasmic reticulum calcium ATPase